Title
POLARIZATION OF SINGLE PARTICLE STATES IN HEAVY ION INDUCED NUCLEAR REACTIONS WITHIN THE TWO CENTER SHELL MODEL

Author
Pruess, K.

Publication Date
1976-08-01

Submitted to Nuclear Physics

LBL-5066
Preprint

POLARIZATION OF SINGLE PARTICLE STATES IN HEAVY ION INDUCED NUCLEAR REACTIONS WITHIN THE TWO CENTER SHELL MODEL

K. Pruess

August 1976

Prepared for the U. S. Energy Research and Development Administration under Contract W-7405-ENG-48

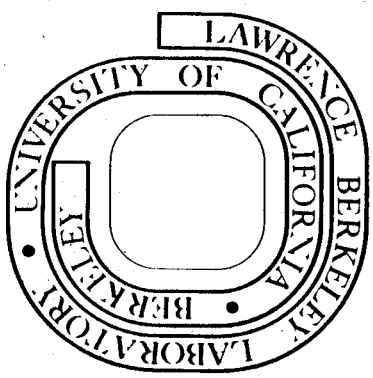

DISCLAIMER

Polarization of Single Particle States in Heavy Ion Induced Nuclear Reactions within the Two Center Shell Model

K. Pruess*

Lawrence Berkeley Laboratory

University of California

Berkeley, Cal., 94720

---

* Fellow of Deutscher Akademischer Austauschdienst, Bonn; supported by U.S. Energy Research and Development Administration.

Abstract.

In "slow" nucleus-nucleus collisions the single particle states will adjust continuously to an instantaneous two center potential. Transfer reactions will occur between polarized rather than between asymptotic states.

In order to employ two center states in reaction calculations, an expansion in terms of asymptotic states with good angular momentum is required. This expansion is formulated, and equations for the expansion coefficients are derived. Model calculations for the system $^{40}Ca + ^{16}O$ indicate that the polarization of unoccupied proton states in ^{40}Ca is strong, while it is very weak for the tightly bound $1p_{1/2}$ - proton in ^{16}O. The dependence of the polarization effect on several relevant parameters is discussed.

I. Introduction.

Two center shell models, using either pre-given or self-consistent (constrained Hartree-Fock) potentials, have been applied to problems of nuclear fission and nucleus-nucleus collisions for quite some time.[1-10] More specifically, these models have been used for the microscopic calculation of total energies of nuclear configurations, which depend upon a number of collective geometrical parameters (such as shape, fragmentation, length or nucleus-nucleus separation). The resulting potential energy surfaces (PES) were taken as potentials governing collective modes of motion, such as the elongation and necking in of a fissioning nucleus, or the relative motion of two colliding nuclei.

Underlying these models is an adiabatic picture, with the single particle motion considered to be fast compared to the collective motion. If this is to be taken seriously, and consistently, then not only the single particle energies would adjust to the collective motion. Also, single particle wave functions should be taken to depend upon collective variables as parameters. E.g. in nucleus-nucleus collisions the internal motion should not be described with the asymptotic states of the free separated nuclei. If an adiabatic picture applies, all single particle states would adjust continuously to the approaching shell model potential of the other nucleus.[9] At any nucleus-nucleus distance the nucleons would occupy instantaneous two center states rather than asymptotic states. Rearrangement reactions will occur between instantaneous polarized (two center) single particle states, with form factors presumably rather different than for asymptotic states. The phenomenological description of elastic scattering is not affected, of course, because all

internal degrees of freedom can be integrated out.

In an actual scattering experiment, the polarization of single particle states will be less than predicted for the adiabatic limit. It depends upon the ratio of transit time to nuclear period, which can be estimated as $(E_{Fermi}/(E/A))^{1/2}$. For $E_{Fermi} \sim 30$ MeV and the collision energy per projectile nucleon E/A typically of the order of 5 MeV, this ratio will be $\sqrt{6}$, which is large but not very large compared to 1. Qualitatively, we expect that the polarization effect will increase both the interaction radius and the diffuseness of the interaction region. This effect will become stronger with increasing excitation of the participating states. It will shift grazing peaks in transfer angular distributions forward, and will enhance transfer at forward angles.

Experimental evidence for this, and actual reaction calculations employing polarized single particle states, are reported elsewhere.[11] In this paper we shall discuss the technique through which parameter dependent channel functions, calculated within the two center shell model, may be employed in reaction calculations. The essential step is to expand two center states in terms of asymptotic states of free nuclei. Formulas for the coefficients of the 'asymptotic expansion' are given in ch. III. We also present some model calculations and discuss systematics of the polarization effect.

Although our method is generally applicable to any two center models, including self-consistent ones, the actual discussion will be based on the model as developped by Maruhn and Greiner.[6]

II. The Model.

We use the asymmetric two center shell model (TCSM) in the form as developped by Maruhn and Greiner.[6] For the definition of the Hamiltonian and the calculation of the eigenstates we refer the reader to their paper. The potential is a modified asymmetric two center oscillator, including the usual $\underset{\sim}{\ell}\cdot\underset{\sim}{s}$ and $\underset{\sim}{\ell}^2$-forces. To avoid the unphysical sharp cusp appearing in the two center oscillator, the potential between the centers is represented by a polynomial of fourth degree. The height of the potential barrier between the nuclei may be chosen freely. While from a physical point of view it would be preferable to use a two-center Woods-Saxon potential, the Maruhn/Greiner model has the advantage that all potential matrix elements can be evaluated analytically in a suitably chosen basis (see below). Also, the shape of the barrier region can be made to quite closely resemble that of a two center Woods-Saxon potential (see fig. 1).

The TCSM-eigenstates are obtained by numerically diagonalizing the two center Hamiltonian on the basis of the eigenstates of the two center oscillator. The only integrals of motion are energy E and, for collisions of spherical nuclei, projection Ω of the angular momentum on the z-axis (intrinsic symmetry axis). The TCSM-states may be either specified with the quantum numbers E and Ω, or with the (asymptotic) quantum numbers $n\ell j\Omega$ of eigenstates of the spherical harmonic oscillator including $\underset{\sim}{\ell}\cdot\underset{\sim}{s}$-force, which they approach as the two center separation parameter $R \to \infty$.

Thus we have two center single particle states in the form $(\Omega > 0)$

$$|E\Omega\rangle \equiv |Rn\ell j\Omega\rangle$$

$$= \sum_{n_z n_\varsigma} \left(a^{n\ell j\Omega\uparrow}_{n_z n_\varsigma}(R) |n_z n_\varsigma\ \Omega-\tfrac{1}{2}\rangle \chi_{\frac{1}{2}} + a^{n\ell j\Omega\downarrow}_{n_z n_\varsigma}(R) |n_z n_\varsigma\ \Omega+\tfrac{1}{2}\rangle \chi_{-\frac{1}{2}} \right) \qquad (1)$$

where we have introduced an obvious notation for spin-up and spin-down components. χ_μ is a spin function. The $|n_z n_\varsigma m\rangle$ are eigenstates of the two center oscillator (see appendix A).

It is not obvious how single particle states of the form eq. (1) should be used in the calculation of rearrangement reactions. They depend upon the nucleus-nucleus distance as a parameter, thereby abandoning the rigorous separation of internal and relative motion. Additional kinetic energy terms would arise from the parametric dependence. However, the variation of the state eq. (1) as a function of R will be small in the region where quasielastic reactions proceed, so that for these the additional kinetic terms may well be negligible in comparison with the kinetic terms from the radial motion proper. A more basic difficulty concerns the connection between the TCSM separation parameter R and a relative motion coordinate for the nucleus-nucleus system. The usual description of relative motion employs the vector $\underset{\sim}{r}_\alpha$ connecting the mass centers of a particular (arbitrary but fixed) partition $\alpha = (A_\alpha, B_\alpha)$ of the $A = A_\alpha + B_\alpha$ nucleon system, $\underset{\sim}{r}_\alpha = \sum_{i\in A_\alpha} \underset{\sim}{r}_i / A_\alpha - \sum_{i\in B_\alpha} \underset{\sim}{r}_i / B_\alpha$. Strictly speaking, it should not be the length r_α of this vector

upon which the polarization of single particle states should be considered to depend. If two nuclei could be placed next to each other at e.g. a distance typical of grazing collisions, all single particle states would be polarized in a certain way. The Pauli principle would require all partitions to be present, not just the one distinguished in the definition of $\underset{\sim}{r}_\alpha$. Each partition would correspond to a different value of r_α for a fixed nucleus-nucleus configuration. The separation parameter R, which determines the radial dependence of the polarization in our model, should rather be connected with a symmetrical distance coordinate, which is invariant with respect to nucleon permutations and depends only upon the geometry of the nucleus-nucleus system.

A description of nucleus-nucleus collisions in terms of symmetrical relative motion coordinates, including Euler angles for the relative angular motion, has been formulated in ref. 12 . However, a solution to the equations of motion which would allow actual reaction calculations has not yet been accomplished.

For the time being one may use reaction theories such as the DWBA or coupled channel formalisms, and identify $R \simeq r_\alpha$ in the spirit of a particle-core picture. In order to take the polarization effect into account all asymptotic single particle states have to be replaced according to

$$|n\ell_j\Omega\rangle \Psi^{(\pm)}_{(\underset{\sim}{r}_\beta)} \longrightarrow |\underset{\sim}{r}_\alpha(=R) n\ell_j\Omega\rangle \Psi^{(\pm)}_{(\underset{\sim}{r}_\beta)} \qquad (2)$$

where $\Psi^{(\pm)}$ is the function of relative motion (e.g. distorted wave). The usual reaction theories require angular momentum coupling of internal and relative motion. As the polarized state, eq. (1) , contains a superposition of

many states with different angular momenta, it must be decomposed in terms of asymptotic states with good angular momentum.

$$|Rn\ell j\Omega\rangle = \sum_{n'\ell'j'} A^{n\ell j\Omega}_{n'\ell'j'}(R)\,|n'\ell'j'\Omega\rangle \qquad (3)$$

The asymptotic states $|n'\ell'j'\Omega\rangle$ may be either those of nucleus 1 or, at a distance R apart, those of nucleus 2 (see below).

We shall refer to eq. (3) as an 'asymptotic expansion'. The actual calculation of this for a two center state of the form eq. (1) is the main objective of this paper.

The polarization coefficients have the following asymptotic behaviour

$$A^{n\ell j\Omega}_{n'\ell'j'}(R) \underset{R\to\infty}{\sim} \delta_{nn'}\,\delta_{\ell\ell'}\,\delta_{jj'} \qquad (4)$$

Taking polarization into account amounts to having a very large number of virtual channels $(n'\ell'j')$ present (of the order of 100 in typical cases, as we shall see). These channels are off the energy shell, and hence are confined to the interaction region, cf. eq. (4). In principle, all virtual channels have to be treated explicitly by means of coupled equations, very much like strong inelastic channels. Transfer between polarized single particle states would appear as indirect processes with a large number ($\sim$100) of virtual channels as intermediaries. Usually, indirect contributions to transfer via a large number of weak states are neglected on the basis of a random phase argument. Such an argument is not applicable in the case of nucleus-nucleus polarization, however, because the coherence is strong

(see below). The TCSM may be regarded as a natural way to approximately parameterize the distance-dependent admixture of virtual states, thereby avoiding a very large coupled channels problem in the subspace of closed channels.

If a description of relative motion in terms of symmetrical coordinates would actually be feasible, no asymptotic expansion eq. (3) would be needed for reaction calculations with polarized particle states. The TCSM-states as given by eq. (1) could be used directly in the evaluation of transfer form factors, without explicit recourse to virtual channels. This desirable simplification would occur because the Euler angles would carry not just the relative, but the total angular momentum. An expansion in terms of asymptotic states remains useful, however, because it provides insight into the polarization effect (cf. ch. IV).

III. The Asymptotic Expansion.

To obtain the two center state eq. (1) in the form of an asymptotic expansion, eq. (3), the states $|n_z n_\varsigma m\rangle \chi_\mu$ $(m + \mu = \Omega)$ must be expanded in terms of states $|n' \ell' j' \Omega\rangle$. This is done in three steps. First, the z-part of the two center oscillator states is expanded in terms of harmonic oscillator states (see appendix A):

$$|n_z\rangle = \sum_{\hat{n}} h_{\hat{n}}^{n_z} |\hat{n}\rangle \qquad (5)$$

Then the states $|\hat{n}\, n_\varsigma m\rangle$ are expanded in terms of eigenstates of $\underset{\sim}{\ell}^2$. In order to facilitate this expansion, we choose the ς-frequency ω_ς of the two center oscillator basis functions to be equal to the z-frequency ω_1 or ω_2, depending

upon whether we want to expand on asymptotic states of nucleus 1 or nucleus 2 (see appendix B). With the indicated choice of ω_ζ, the $|\hat{n}\, n_\zeta m\rangle$ are eigenstates of the spherically symmetric harmonic oscillator, written in a cylindrical basis. The $\underset{\sim}{\ell}^2$-expansion is written

$$|\hat{n}\, n_\zeta m\rangle = \sum_{\ell'} C^{\hat{n}}_{\ell'}(N', m)\, |n'\ell' m\rangle \tag{6}$$

where

$$N' = \hat{n} + 2n_\zeta + |m| = 2n' + \ell' \tag{6a}$$

is the phonon number. The calculation of the coefficients $C^{\hat{n}}_{\ell'}$ is discussed in appendix B.

Finally, we expand in terms of total angular momentum eigenstates:

$$\langle\vartheta\varphi|\ell' m\rangle\chi_\mu \equiv Y_{\ell m}(\vartheta\varphi)\,\chi_\mu = \sum_{j'\Omega} C^{m\mu\Omega}_{\ell' s j'}\, |\ell' j' \Omega\rangle \tag{7}$$

Using the explicit forms for the Clebsch-Gordon coefficients we find for the polarization amplitudes in eq. (3) (for $\Omega > 0$)

$$A^{n\ell j\Omega}_{n'\ell' j'_>}(R) = \sum_{n_z n_\zeta} \left\{ \left(\frac{\ell'+\Omega+\frac{1}{2}}{2\ell'+1}\right)^{1/2} a^{n\ell j\Omega\uparrow}_{n_z n_\zeta}(R)\, h^{n_z}_{N'-2n_\zeta-\Omega+\frac{1}{2}}\, C^{N'-2n_\zeta-\Omega+\frac{1}{2}}_{\ell'}(N', \Omega-\tfrac{1}{2}) \right.$$
$$\left. + \left(\frac{\ell'-\Omega+\frac{1}{2}}{2\ell'+1}\right)^{1/2} a^{n\ell j\Omega\downarrow}_{n_z n_\zeta}(R)\, h^{n_z}_{N'-2n_\zeta-\Omega-\frac{1}{2}}\, C^{N'-2n_\zeta-\Omega-\frac{1}{2}}_{\ell'}(N', \Omega+\tfrac{1}{2}) \right\} \tag{8a}$$

where $\qquad N' = 2n' + \ell' \,; \qquad j'_> = \ell' + \tfrac{1}{2}$

$$A^{n\ell_j\Omega}_{n'\ell'_{j'<}}(R) = \sum_{n_z n_\varsigma} \left\{ \left(\frac{\ell'+\Omega+1/2}{2\ell'+1}\right)^{1/2} a^{n\ell_j\Omega\downarrow}_{n_z n_\varsigma}(R)\, h^{n_z}_{N'-2n_\varsigma-\Omega-1/2}\, C^{N'-2n_\varsigma-\Omega-1/2}_{\ell'}(N', \Omega+1/2) \right.$$

$$\left. -\left(\frac{\ell'-\Omega+1/2}{2\ell'+1}\right)^{1/2} a^{n\ell_j\Omega\uparrow}_{n_z n_\varsigma}(R)\, h^{n_z}_{N'-2n_\varsigma-\Omega+1/2}\, C^{N'-2n_\varsigma-\Omega+1/2}_{\ell'}(N', \Omega-1/2) \right\} \quad (8b)$$

where $N' = 2n' + \ell'$; $j'_< = \ell' - 1/2$

As the two center oscillator basis states themselves depend upon the two center separation parameter R, the coefficients $h^{n_z}_{\hat{n}}$ are also functions of R (which we have not indicated through an explicit notation).

Matrix elements of the TCSM-Hamiltonian are independent of the sign of Ω. Therefore,

$$A^{n\ell_j-\Omega}_{n'\ell'_{j'}} = A^{n\ell_j\Omega}_{n'\ell'_{j'}} \quad (8c)$$

For purposes of discussing systematics of the polarization effect it is convenient to also consider a first order perturbation expression for the amplitudes $A^{n\ell_j\Omega}_{n'\ell'_{j'}}(R)$. We have[13]

$$A^{n\ell_j\Omega}_{n'\ell'_{j'}}(R) \simeq \frac{\langle n'\ell'_{j'}\Omega | V_R | n\ell_j\Omega\rangle}{E_{n\ell_j} - E_{n'\ell'_{j'}}} \quad (9)$$

Here V_R is the shell model potential of the polarizing nucleus at a distance R. Taking only the momentum-independent parts of V_R into account and using eq. (7) we have

$$A^{n\ell_j\Omega}_{n'\ell'_{j'}}(R) \simeq \left(E_{n\ell_j} - E_{n'\ell'_{j'}}\right)^{-1} \sum_{m\mu} C^{m\mu\Omega}_{\ell s_j} C^{m\mu\Omega}_{\ell' s'_{j'}} \langle R_{n'\ell'} Y_{\ell' m} | V_R | R_{n\ell} Y_{\ell m} \rangle \qquad (10)$$

IV. Results and Discussion.

1. The Calculation.

We have programmed the calculation of eqs. (8) on a CDC 7600 computer. Table I gives a summary of the steps and times involved. The computational procedure has not been optimized yet.

The lengthiest part of the calculation is seen to be the numerical integration (ii) to obtain the $f^{n_z}_{\hat{n}}$, eq. (A.12). This could be avoided altogether, if the diagonalization (i) of the TCSM were made with harmonic oscillator rather than two center oscillator states. Thereby the dimension of the eigenvalue problem (i) would increase by more than a factor of 3, and the required calculation time would increase by a factor of 10 approximately. Thus it appears not to be advantageous to avoid step (ii). It would certainly become a disadvantage if at a fixed R several calculations for different TCSM-barriers were made, requiring several

calculations (i) and only one calculation (ii).

If a different TCSM were considered, e.g. a more realistic two center Woods-Saxon or a self-consistent potential, only calculation (i) would be affected. The a(R) in eq. (1) would be numerically different. All equations given in chs. II, III and in appendices A, B remain valid.

Calculation (iii) has to be made just once and for all, as the coefficients $\hat{c}^{\hat{n}}_{\ell'}(N,m)$, eq. (6), do not depend upon any parameters.

We have restricted ourselves so far to collisions of spherical nuclei. The two center model we use has the following adjustable parameters.

R, the separation between the potential centers;

ε, which measures the barrier height in units of the barrier for a two center oscillator at the same separation;

ω_i (i = 1,2), the frequency parameters of the underlying two center oscillator;

$\varkappa_i$, μ_i (i = 1,2), strength parameters of the $\underset{\sim}{\ell}\cdot\underset{\sim}{s}$ and $\underset{\sim}{\ell}^2$-forces, respectively.

We have adjusted the ω_i to the rms-radii of the colliding nuclei.[2] For the $\varkappa_i$, μ_i the asymptotic values applying to the free separated nuclei were taken.[14] ε was taken to get as close a resemblance to a two center Woods-Saxon potential as possible (see fig. |).

As it is advantageous for certain systematic explorations we have also made calculations with the unmodified two center oscillator form of the barrier region.

To check the accuracy of the calculation, we have numerically compared both sides of eq. (A.10). Using the first fifty oscillator shells we found that the difference between the (one dimensional) two center oscillator function and its harmonic oscillator expansion for $^{40}Ca + ^{16}O$ at R = 10 fm never exceeded 10^{-4} whenever the function (absolute value) exceeded 10^{-1}. This holds for the first 13 two center oscillator states, with the agreement improving for the lower states.

Another check was made with respect to the normalization of the full 3-dimensional polarized state in the form of an asymptotic expansion, eq. (3). Including the first 40 oscillator shells ($N' = 2n' + \ell' \leq 39$) we found that

$$1 - \sum_{n'\ell'j'} \left[A^{n\ell j\Omega}_{n'\ell'j'}(R = 10\,\text{fm}) \right]^2 \lesssim 10^{-7} \qquad (11)$$

for single particle states up to E = 50 MeV (fp - shell) in $^{40}Ca + ^{16}O$ (rounded barrier, $\varepsilon = 0.8$). Even this small difference appears to be "real", i.e. due to the N' - cutoff, as it decreases continuously with decreasing E to below 10^{-9} for the $1s_{1/2}$ ^{40}Ca - state at 16.4 MeV.

A more sensitive check can be made from the normalization of a polarized state, which is expanded on the basis of the polarizing rather than that of the polarized nucleus; the check being more sensitive because the center of the expansion states is displaced by R with respect to the to-be-expanded state. Hence no single component is strong in this case. For the $1p_{1/2}$ -state in ^{16}O e.g., polarized from a ^{40}Ca - nucleus at R = 10 fm distance (rounded barrier, $\varepsilon = 0.8$), no single

$A^{1p^{1/2}1/2}_{n'\ell'j'}$ exceeds 0.14 when the expansion is made in terms of asymptotic ^{40}Ca - states. And yet we find the normalization to be $1 - 3\times10^{-8}$.

The accuracy of the calculation can also be checked from the asymptotic behaviour of the coefficients $A^{n\ell j\Omega}_{n'\ell'j'}(R)$, eq.(4) . For $^{40}Ca + ^{16}O$ and an unmodified two center oscillator barrier we find at R = 14 fm, which is "large",

$$1 - A^{n\ell j\Omega}_{n\ell j}(R=14\,\text{fm}) \lesssim 10^{-6} \qquad (12)$$

for ^{40}Ca - states with $E \lesssim 41$ MeV. (For higher states there is still some polarization present at R = 14 fm, which diminishes the amplitude of the parent state to e.g. $1 - 5\times10^{-5}$ at E = 50 MeV.)

In what follows we shall give a survey of properties of the polarization coefficients $A^{n\ell j\Omega}_{n'\ell'j'}(R)$. The discussion will mainly focus on the system $^{40}Ca + ^{16}O$, with rather obvious generalizations to other systems.

2. General Behaviour of Polarization Amplitudes.

Among the outstanding features of the polarization effect is that it admixes a large number of states with appreciable amplitudes. The $1f_{7/2}\,1/2$ -proton state in ^{41}Sc e.g., which is populated in proton transfer to ^{40}Ca, has admixed about 130 states with amplitudes (absolut value) in excess of 0.02 due to a polarizing ^{16}O -nucleus at grazing distance R = 10 fm.

The polarization amplitudes show marked systematics. More specifically, the $A^{n\ell j\Omega}_{n'\ell'j'}(R)$ are slowly and smoothly varying functions of n' and ℓ', which attain

a number of extrema in different $n'\ell'$ -regions. This suggests a convenient way to present and discuss the large amount of data characterizing the polarization effect. Interpolating between neighbouring values of n' and ℓ' we extend the $A^{n\ell j\Omega}_{n'\ell'j'}(R)$ to a continuous range of $n'\ell'$, and display them in the form of contour maps in the $n'\ell'$ - plane (figs. 2 - 8).

For each single particle state (asymptotic quantum numbers $n\ell j\Omega$), and each nucleus-nucleus distance R, there are two such maps: One for the $j'_> = \ell' + 1/2$ -states, and one for the $j'_< = \ell' - 1/2$ -states. If the polarization coefficients are evaluated up to a certain $N' = 2n' + \ell'$, each map is confined to a triangle. It is convenient to combine both into a single figure, and to choose the scale of the ℓ' -axis half that of the n' -axis. The second main diagonal divides the $j'_>$ - from the $j'_<$ - map. Parallels to this diagonal correspond to states of the same oscillator shell $N' = 2n' + \ell'$, hence the same rms-radius $\langle r^2 \rangle = (N'+3/2)\hbar/m\omega$. The contour maps give a pictorial representation of what a single particle state including polarization effects looks like (figs. 2 - 8).

A general understanding of the polarization effect may be obtained from an inspection of the polarized wave function in 3-dimensional space. Figs. 9-12 show contour maps of the probability density $\psi^*\psi$, calculated from eq. (1) . It is seen that the single particle states are slightly distorted from their asymptotic appearance within the polarized nucleus, and, more important, have attained a whole new region of appreciable amplitudes near the center of the polarizing nucleus.

The smooth and slow variation of the $A^{n\ell j\Omega}_{n'\ell'j'}$ as a function of $n'\ell'$ assures a coherence of the participating states, eq. (3), in a limited region of space near the center of the polarizing nucleus. Each extremum region in the $n'\ell'$ -plane represents a collection of states which interfer with nearly equal amplitudes to give a non-zero wave function in some limited region of space. This can be explicitly seen from fig. 8 which displays the coefficients for the expansion of the $1s_{1/2\ 1/2}$ - state in a ^{16}O - nucleus on the basis of a ^{40}Ca - nucleus at R = 12 fm distance.

To further clarify this coherence it is convenient to expand a polarized state, which asymptotically belongs to a ^{40}Ca - nucleus, on eigenstates of the polarizing ^{16}O - nucleus. Table 2 shows that the polarization essentially consists of admixing a small number of ^{16}O - states with neighbouring single particle energies into the ^{40}Ca - states. It is the representation of these components on a ^{40}Ca - basis at a distance R of the order of 10 fm, which requires expansion coefficients $A^{n\ell j\Omega}_{n'\ell'j'}$ varying slowly and smoothly with $n'\ell'$, as shown in figs. 2-5.

3. Specific Effects.

3.1 R - dependence.

The polarization effect decreases, and ultimately vanishes, with increasing distance R (see eqs. (4),(10)). As a natural measure of the overall strength of the polarization we introduce the total probability accounted for by the admixed states

$$P^{n\ell j\Omega}(R) = \sum_{n'\ell'j'}{}' \left[A^{n\ell j\Omega}_{n'\ell'j'}(R)\right]^2 = 1 - \left(A^{n\ell j\Omega}_{n\ell j}\right)^2 \qquad (13)$$

The prime at the sum indicates that $(n'\ell'j') \neq (n\ell j)$. From fig. 13 it is seen that P(R) typically decreases by an order of magnitude for an increase in the ^{40}Ca - ^{16}O distance by 1 fm.

In fig. 14 we have depicted a number of polarization amplitudes as a function of R. While asymptotically they all approach zero, their radial dependence appears to be rather different in the grazing region (around R = 10 fm). Looking at the polarized wave function in 3-dimensional space we see (fig. 9) that the admixtures are localized near the center of the polarizing nucleus. They move with this nucleus when R varies. At the same time they decrease with increasing R, while preserving their general shape. It is this interplay of two effects, which makes the R-dependence of the A appear complicated, which in fact it is not.

Firstly, upon letting R increase all contours of $A^{n\ell j\,\Omega}_{n'\ell'j'}(R)$ in the $n'\ell'$ - plane move outward, towards greater $n'\ell'$ (see fig. 2 and table 3). This merely reflects the fact that states with larger rms - radius $\langle r^2\rangle_{N'} \sim N'$ are needed to represent the admixtures near the center of the polarizing nucleus when the latter moves away. Secondly, all coefficients in an extremum region decrease in a similar fashion when R increases, so that the shape of the polarization contour map and of the interference pattern in space persist. This property suggests useful approximations for practical applications (reaction calculations), so that we will explore it in some detail.

Accounting explicitly for the R - dependent shift in extrema locations we postulate an R - dependence of the polarization amplitudes which is independent of the

admixed states. Labelling the latter with $n_i \ell_i j_i$ instead of $n'\ell'j'$ we write

$$A^{n\ell j\Omega}_{n_i\ell_i j_i}(R) \approx f^{n\ell j\Omega}_{R_0}(R)\, A^{n\ell j\Omega}_{n_i(R)\ell_i(R)j_i(R)}(R_0) \qquad (14)$$

$$(n_i\ell_i j_i) \neq (n\ell j)$$

We adopt the convention, once and for all, to take $R_0 = 10$ fm as a reference, and will henceforth drop it notationally.

We shall now show that eq. (14), to a good approximation, indeed gives a consistent representation of the R - dependence. f may be determined from normalization arguments, in the following way. Introducing the abbreviation

$$A^{n\ell j\Omega}_{n_i\ell_i j_i}(R) = A_i(R) \qquad (15)$$

we have, using eq. (14)

$$A_0(R)^2 + \sum_i{}' A_i(R)^2 = A_0(R)^2 + f(R)^2 \sum_i{}' A_i(R=10\text{fm})^2$$

$$= 1 = A_0(R=10)^2 + \sum_i{}' A_i(R=10)^2 \qquad (16)$$

so that

$$f^{n\ell j\Omega}(R) = \sqrt{\frac{1-A_0(R)^2}{1-A_0(10)^2}} = \sqrt{\frac{P^{n\ell j\Omega}(R)}{P^{n\ell j\Omega}(10)}} \qquad (17)$$

Table 3 gives as an example values of $f^{1f_{7/2}1/2}(R)$ for the system $^{40}Ca + ^{16}O$. In order to check the hypothesis of "persistent shape" of the polarization contour map, which we have formulated in eq. (14), we may directly calculate f from eq. (14), comparing "corresponding" polarization amplitudes at different R. "Corresponding" amplitudes may be found at "corresponding" extrema. We have listed the pertinent quantities in table 3. It is seen that the ratios of A's for different extrema are fairly close. Part of the deviations may be attributed to the fact that the $A^{nlj\Omega}_{n_i l_i j_i}$ are confined to integral values of $n_i l_i$, which may coincide more or less closely with extrema in a continuous map.

The $f(R)$ as determined from amplitudes at extrema compares well with that calculated from eq. (17). It is seen, however, that for R < 10 (reference distance) eq. (17) underestimates and for R > 10 overestimates amplitudes at extrema. This can be understood from the fact that with increasing R in general all structures in the polarization contour map become somewhat wider, i.e. the number of states contained within corresponding contours increases slightly. This effect is neglected in eq. (14). We conclude that, with this approximation, eqs. (14), (17) give a consistent description of the radial dependence of the polarization.*

3.2 Ω - dependence.

Polarization effects generally are largest for $|\Omega| = 1/2$ and decrease fast with increasing $|\Omega|$. In a typical situation ($1f_{7/2}$ - state around a ^{40}Ca - core, ^{16}O at grazing distance R = 10 fm) the polarization decreases by roughly an order of magnitude if $|\Omega|$ increases by 1 (see fig. 13).

* Because of the schematic form of the barrier in our two center model (see fig. 1), and because of the neglect of Coulomb effects, the R-dependence of the polarization as determined in this work is probably not realistic.

This feature is of purely geometric origin and can be understood from the first order perturbation expression, eq. (10). The polarizing potential V_R is centered on the z-axis, i.e. around $\vartheta = 0$ as seen from the ^{40}Ca - nucleus. For $m \neq 0$ $Y_{\ell m}$ is proportional to $(1 - \cos^2\vartheta)^{m/2}$. Only for $|\Omega| = 1/2$ does an angular function $Y_{\ell m}$ with $m = 0$, which is non-zero on the z-axis, appear in the matrix element of eq. (10). For a given ℓ the region around $\vartheta = 0$ in which $Y_{\ell\, |\Omega| - \frac{1}{2}}$ is small increases with $|\Omega|$. The asymptotic state reaches the perturbing potential only at small R, at which part of the perturbing potential is seen under a large angle ϑ.

It is suggested that for quasielastic reactions the polarization effect need only be taken into account for the $|\Omega| = 1/2$ - components.

3.3 E - dependence.

From the perturbation expression eq. (10) it is also clear that polarization effects generally will increase with increasing excitation energy of the single particle states involved, because for higher lying states the tails of the asymptotic wave function reach further out.

In fig. 15 we have depicted the polarization as a function of the single particle energy. It is seen that it increases roughly by an order of magnitude in going to the next major shell. Superimposed on this general trend are resonance effects. When the energy difference between single particle states in the colliding nuclei is small, these states are mutually strongly polarized. In fact, from table 2 it is seen that the polarization essentially consists in admixing a few states

of the polarizing nucleus which have neighbouring energies.

This behaviour is somewhat reminiscent of the resonance mechanism which occurs in elastic scattering involving identical cores.[15] The latter may be considered as a particular case of very strong polarization. Single particle states in a symmetrical two center potential have equal amplitudes in both nuclei (except possibly for the sign). They are not concentrated in one nucleus even asymptotically. The connection between resonance exchange and the polarization effect in general deserves further study in the future.

The above stated resonance behaviour suggests favorable conditions to observe polarization effects experimentally (i.e. to observe discrepancies between DWBA and experimental angular distributions for transfer reactions, which can not be attributed to two step transfer via strong inelastic states). For simplicity consider a one neutron transfer reaction

$$A(a,b)B \quad ; \quad a = b + 1 \quad ; \quad B = A + 1$$

In a particle-core picture, neglecting rearrangement effects, (mutual) resonance polarization will occur for states $|a\rangle = |b\rangle |1\rangle$ and states $|B\rangle = |A\rangle |1\rangle$ if the single particle separation energies fulfill $E_a \approx E_B$.

3.4 Energy Shifts.

Apart from changing single particle wave functions the polarization also makes the single particle energies dependent upon the nucleus-nucleus distance. The energy shift

$$E^{n\ell j\Omega}(R) - E^{n\ell j\Omega}(\infty) \qquad (18)$$

has to be accounted for by the relative motion energy. It acts as an addition to the optical potential $\mathcal{V}(R)+i\mathcal{W}(R)$, which governs the relative motion.

Figure 16 shows that the energy shifts induced by a ^{16}O - nucleus are small ($\sim$ 100 keV) and probably negligible for low lying unoccupied proton states in ^{40}Ca, which might be populated through proton transfer from ^{16}O.

In the case of two identical cores even small energy shifts are not negligible, because they give rise to a peculiar interference effect (resonance exchange).[15]

V. Conclusion.

For collision energies not too high above the Coulomb barrier, polarization of ^{41}Sc - states, which are populated in the proton transfer reaction $^{40}Ca(^{16}O,^{15}N)^{41}Sc$, will be strong (20 % and more). Calculations of angular distributions for this reaction, using polarized single particle states, are under way.

The polarization of states in ^{16}O, on the other hand, is found to be weak ($\sim$ 1 % or less), due to the strong binding of the closed shells. Calculations for other systems (including $^{64}Ni + ^{16}O$, $^{208}Pb + ^{16}O$), which are not presented here, indicate that in grazing collisions ^{16}O - states generally are weakly polarized ($\sim$ 1 % or less), whereas states populated in transfer to the heavy nucleus are strongly polarized ($\sim$ 20 % and more).

We find that the polarization is sensitive to the shape of the potential barrier between the nuclei. Therefore, calculations with realistic two center models (Woods-Saxon or self-consistent) are desirable. Such calculations, taking into account also Coulomb effects, are in progress.[22]

Acknowledgement.

The hospitality of the Nuclear Theory Group in the Lawrence Berkeley Laboratory and discussions with N.K. Glendenning, G. Delic, and L.A. Charlton are gratefully acknowledged. Special thanks go to N.K. Glendenning for a critical reading of the manuscript and valuable suggestions. Advice on the numerical calculations from the staff of the LBL - computer center, and especially T. Clements, has been very helpful.

Appendix A: One - and two - center Oscillator.

Consider a one - dimensional harmonic oscillator, centered at z_λ

$$V_\lambda(z) = \frac{1}{2} m \omega_\lambda^2 (z - z_\lambda)^2 \qquad (A.1)$$

$\lambda = 1,2$ specifies the nucleus to which the potential corresponds.

For our purposes it is convenient to write eigenstates of the potential eq. (A.1) in terms of parabolic cylinder functions rather than in terms of the more customary Hermite polynomials.[16]

$$\varphi_n^\lambda(z) = M_\lambda^{-1} \, U(-n-\tfrac{1}{2}, x_\lambda) \qquad (A.2)$$

where

$$M_\lambda = \left(\frac{\pi}{k_\lambda}\right)^{1/4} \sqrt{n!} \qquad (A.3a)$$

$$k_\lambda = m\omega_\lambda/\hbar \qquad (A.3b)$$

$$x_\lambda = \sqrt{2k_\lambda}\,(z - z_\lambda) \qquad (A.3c)$$

A one - dimensional two center oscillator potential may be written as

$$V_{TCOSM}(z) = \frac{m}{2} \cdot \begin{cases} \omega_1^2 (z-z_1)^2 & \text{if } z \le 0 \\ \omega_2^2 (z-z_2)^2 & \text{if } z \ge 0 \end{cases} \qquad (A.4)$$

where

$$\omega_1^2 z_1^2 = \omega_2^2 z_2^2 \tag{A.4a}$$

to assure continuity.

Eigenstates of the potential eq. (A.4)) may also be expressed in terms of parabolic cylinder functions.[6]

$$\varphi_{n_z}(z) = N_\sigma^{-1} \, U(-n_{z_\sigma} - \tfrac{1}{2}, (-)^\sigma x_\sigma) \tag{A.5}$$

where

$$\sigma = \frac{\operatorname{sgn} z + 3}{2} \tag{A.5a}$$

The quantum numbers n_{z_σ} and the normalization N_σ have to be calculated numerically. For reference purposes we also give the eigenstates $|n_z n_\varrho m\rangle$ of the 3 -dimensional two center oscillator with potential energy

$$V(\varrho, z) = \frac{m}{2} \omega_\varrho^2 \varrho^2 + V_{TCOSM}(z) \tag{A.6}$$

We have[6]

$$\langle z \varrho \varphi | n_z n_\varrho m \rangle = \varphi_{n_z}(z) \, \chi_{n_\varrho}^{|m|}(\varrho) \, \eta_m(\varphi) \tag{A.7}$$

where $\varphi_{n_z}(z)$ is given by eq. (A.5) and

$$\chi_{n_\varrho}^{|m|}(\varrho) = \sqrt{\frac{2 n_\varrho!}{(n_\varrho + |m|)!}} \, k_\varrho^{\frac{|m|+1}{2}} \exp\left(-\frac{k_\varrho}{2} \varrho^2\right) \varrho^{|m|} L_{n_\varrho}^{|m|}(k_\varrho \varrho^2) \tag{A.8}$$

$$(k_\varrho = m \omega_\varrho / \hbar)$$

$$\eta_m(\varphi) = (-)^{\frac{m+|m|}{2}} \frac{e^{im\varphi}}{\sqrt{2\pi}} \tag{A.9}$$

The $L^{|m|}_{n_\rho}$ is a generalized Laguerre polynomial, as defined in ref. 16 . The phase factor in η_m is chosen for convenience.

Eigenstates of the 3 - dimensional spherically symmetric harmonic oscillator in a cylindrical basis may also be written in the form eq. (A.7) except that φ_{n_z} is to be replaced with a harmonic oscillator function, eq. (A.2).

The two center oscillator function eq. (A.5) may be expanded in terms of a complete set of harmonic oscillator states

$$\varphi_{n_z}(z) = \sum_n h^{n_z}_{n,\lambda}\, \varphi^\lambda_n(z) \qquad (A.10)$$

where $\lambda = 1$ or 2, depending upon whether one wants to expand after states of nucleus 1 or 2.

Introducing

$$\mu = \lambda - (-)^\lambda = \begin{cases} 2 & \text{if } \lambda = 1 \\ 1 & \text{if } \lambda = 2 \end{cases} \qquad (A.11)$$

we have

$$h^{n_z}_{n,\lambda} = \int_{-\infty}^{\infty} dz\, \varphi^\lambda_n(z)\, \varphi_{n_z}(z)$$

$$= \frac{(-)^{n\cdot\lambda}\,(M_\lambda N_\lambda)^{-1}}{\sqrt{2k_\lambda}\,(n-n_{z_\lambda})}\Big[U(-n_{z_\lambda}-\tfrac{3}{2},q_\lambda)\,U(-n-\tfrac{1}{2},q_\lambda) - U(-n-\tfrac{3}{2},q_\lambda)\,U(-n_{z_\lambda}-\tfrac{1}{2},q_\lambda)\Big]$$

$$+ \frac{(-)^{n\cdot\mu}\,(M_\lambda N_\mu)^{-1}}{\sqrt{2k_\mu}} \int_{q_\mu}^{\infty} dx_\mu\, U\Big(-n-\tfrac{1}{2},\sqrt{2k_\lambda}\Big[\frac{x_\mu}{\sqrt{2k_\mu}}+z_2-z_1\Big]\Big)\, U(-n_{z_\mu}-\tfrac{1}{2},x_\mu)$$

(A.12)

where

$$q_\lambda = (-)^\mu \sqrt{2k_\lambda}\, z_\lambda \qquad (\lambda,\mu) = (1,2),(2,1) \tag{A.13}$$

The first term in eq. (A.12) is an analytical expression for that part of the overlap integral in which the parabolic cylinder functions of two center - and harmonic - oscillator states depend upon the same argument.[6] The second integral must be evaluated numerically.

Appendix B: Angular Momentum Eigenstates in a Cylindrical Basis.

We start from eigenstates of the spherically symmetric harmonic oscillator, written in a cylindrical basis as $|\hat{n}\, n_\varsigma\, m\rangle$. Eigenstates of $\underset{\sim}{\ell}^2$, written as

$$|n'\ell'm\rangle = \sum_{\hat{n}} C^{\hat{n}}_{\ell'}(N',m)\, |\hat{n}\, n_\varsigma\, m\rangle \tag{B.1}$$

may be formed as a linear combination of states with the same phonon number

$$N' = \hat{n} + 2n_\varsigma + |m| = 2n' + \ell' \tag{B.2}$$

Requiring the state eq. (B.1) to in fact be an eigenstate of $\underset{\sim}{\ell}^2$ gives the following eigenvalue equation *

$$\sum_{\hat{n}} C^{\hat{n}}_{\ell'}(N',m)\Big[\langle \hat{n}'\, n'_\varsigma\, m|\, \underset{\sim}{\ell}^2\, |\hat{n}\, n_\varsigma\, m\rangle - \hbar^2 \ell(\ell+1)\, \delta_{\hat{n}'\hat{n}}\, \delta_{n'_\varsigma n_\varsigma}\Big] = 0 \tag{B.3}$$

where

$$\hat{n}' + 2n'_\varsigma + |m| = \hat{n} + 2n_\varsigma + |m| = N' \tag{B.4}$$

* The author is indebted to Dr. P. Lichtner who, after completion of this work, brought to his attention a paper by J.D. Talman.[23] Talman derives an analytical expression for the coefficients $C^{\hat{n}}_{\ell'}(N',m)$, which could be used instead of going through the eigenvalue problem eq. (B.3).

The solution of eq. (B.3) involves, for each phonon number N' and each $\underset{\sim}{\ell}$ -projection m separately, diagonalization of the matrix of $\underset{\sim}{\ell}^2$ in a cylindrical basis.

The matrix elements of $\underset{\sim}{\ell}^2$ are computed from the formulas given in ref. 4 in a straightforward way. Introducing

$$N_\varsigma = 2n_\varsigma + |m| \tag{B.5}$$

we find

$$\begin{aligned}\langle \hat{n}'\, N_\varsigma'\, m' | \underset{\sim}{\ell}^2 | \hat{n}\, N_\varsigma\, m \rangle &= \hbar^2 \delta_{m'm} \Big[\sqrt{(N_\varsigma^2 - m^2)(\hat{n}+1)(\hat{n}+2)}\; \delta_{N_\varsigma'+1\, N_\varsigma-1}\; \delta_{\hat{n}'-1\, \hat{n}+1} \\ &\quad + (2\hat{n}(N_\varsigma+1) + N_\varsigma + m^2)\; \delta_{N_\varsigma' N_\varsigma}\; \delta_{\hat{n}'\hat{n}} \\ &\quad + \sqrt{(N_\varsigma'^2 - m^2)(\hat{n}'+1)(\hat{n}'+2)}\; \delta_{N_\varsigma+1\, N_\varsigma'-1}\; \delta_{\hat{n}-1\, \hat{n}'+1} \Big]\end{aligned} \tag{B.6}$$

Some care must be exercised in adjusting the phases of the $c^{\hat{n}}_{\ell'}$. The radial part of the spherical states

$$\langle r\vartheta\varphi | n'\ell' m \rangle = R_{n'\ell'}(r)\, Y_{\ell' m}(\vartheta\varphi) \tag{B.7}$$

is taken to be positive at large r, i.e.

$$R_{n'\ell'}(r) = (-)^{n'} N_{n'\ell'} \exp\left(-\frac{m\omega}{2\hbar} r^2\right) r^{\ell'} \; {}_1F_1\left(-n', \ell'+3/2, \frac{m\omega}{\hbar} r^2\right) \qquad (B.8)$$

$$N_{n'\ell'} = \left(\frac{m\omega}{\hbar}\right)^{\frac{2\ell'+3}{4}} \left(\frac{2\,\Gamma(n'+\ell'+3/2)}{n'!}\right)^{1/2} \Big/ \Gamma(\ell'+3/2) \qquad (B.8a)$$

For the $Y_{\ell' m}$ the usual phase convention is adopted, see e.g. ref. 13.

The proper phase of the linear combination eq. (B.1) may be ensured by considering both the region of large r and $\vartheta \to 0$, and, equivalently, the region of large z and $\varsigma \to 0$.

From the explicit form of the spherical harmonics it is easily seen that (discarding the $e^{im\varphi}$ - part)

$$\operatorname{sgn} Y_{\ell' m}(\vartheta \to 0) = (-)^m \qquad (B.9)$$

From eqs. (A.2,8) we have

$$\operatorname{sgn} \varphi_{\hat{n}}(z) = +1 \qquad \text{for large } z \qquad (B.10a)$$

$$\operatorname{sgn} \chi^{|m|}_{n_\varsigma}(\varsigma) = +1 \qquad \text{for small } \varsigma \qquad (B.10b)$$

The important point to appreciate is that the large - z - region is always dominated by the largest $\hat{n}$ contributing to an $\underset{\sim}{\ell}^2$ - eigenstate in eq. (B.1). Taking into account the phase of the φ - part, eq. (A.9), it follows that the phases

of the eigenvectors of eq. (B.3) must be taken such that the $C^{\hat{n}}_{\ell'}(N',m)$ with the largest $\hat{n}$ for any N',m,ℓ' is positive.

The advantage of taking the ς-frequency ω_ς of the basis states equal to the z - frequency ω_1 or ω_2, depending upon whether we want to expand after asymptotic states of nucleus 1 or nucleus 2, is now apparent. Had we chosen ω_ς differently, e.g. $\omega_\varsigma = (\omega_1+\omega_2)/2$ (which is somewhat preferable from the point of view of diagonalizing the TCSM-Hamiltonian)[6], we would not have the simple selection rule eq. (B.2) for the states appearing in eq. (B.1). Hence all oscillator shells would appear simultaneously in the eigenvalue problem eq. (B.3), instead of just one at a time. Also, the matrix elements of $\underset{\sim}{\ell}^2$, eq. (B.6), would be much more complicated.

Table 1: Computation of a typical case.
($^{40}Ca + {}^{16}O$ at a grazing distance R = 10 fm)

	Calculation	evaluated quantities	remarks	time (sec)
(i)	two center oscillator basis states and diagonalization of TCSM	$n_z(R)$ $a^{n\ell j\Omega}_{n_z n_\zeta}(R)$	100 two center oscillator basis states ($E \leq 92.5$ MeV)	8
(ii)	expansion of z - part of two center oscillator states after harmonic oscillator states	$h^{n_z}_{\hat{n}}$	13 two center oscillator states; 40 harmonic oscillator states Gaussian quadrature	60*
(iii)	angular momentum eigenstates in a cylindrical basis	$c^{\hat{n}}_{\ell'}(N',m)$	$N' = 0, \ldots, 39$ $m = 0, \ldots, 6$	10
(iv)	asymptotic expansion	$A^{n\ell j\Omega}_{n'\ell'j'}(R)$	40 single particle states ($E \leq 58$ MeV) $2n' + \ell' \leq 39$	16

* Includes numerical evaluation of both sides of eq. (A.10) for $-20\,\text{fm} \leq z \leq 20\,\text{fm}$ in steps of 0.5 fm as a check of numerical accuracy.

Table 2: Polarization of ^{40}Ca - states due to ^{16}O at grazing distance R = 10 fm.

^{40}Ca - states		^{16}O - states					
$n\ell_j$	$P^{n\ell_j}$	$1d_{5/2}$	$2s_{1/2}$	$1d_{3/2}$	$1f_{7/2}$	$2p_{3/2}$	$\sum A_i^2$
$E_{n\ell_j}$ (MeV)	(10^{-2})	43.43	45.51	48.63	55.39	57.47	(10^{-2})
$1d_{3/2}$ 40.76	4.4	-0.21	-0.09	0.04			5.4
$1f_{7/2}$ 46.43	20.1	0.11	0.27	0.39	0.06		24.1
$2p_{3/2}$ 48.17	41.4		0.11	0.64	0.07		42.7
$2p_{1/2}$ 50.79	8.7			0.09	-0.22	-0.17	8.5
$1f_{5/2}$ 52.53	12.7			0.02	-0.32	-0.15	12.5

The first column lists asymptotic quantum numbers and energies of ^{40}Ca - states for the oscillator shell model. The second column shows the polarization of the $\Omega = 1/2$ components of these states (rounded barrier, $\varepsilon = 0.8$). The amplitudes of strong ^{16}O - components of the polarized states are given in the next five columns. The last column shows the combined probability of the strong ^{16}O - components. Resonance effects are clearly visible, especially for the $1f_{7/2}$ - and $2p_{3/2}$ -states.

Table 3: Dependence of Polarization on Nucleus-Nucleus Distance.

R (fm)	Extrema of $A^{1f_{7/2}\,1/2}_{n'\ell'j'}(R)$ $j'>$ 1. (a)	1. (b)	2. (a)	2. (b)	3. (a)	3. (b)	$j'<$ 4. (a)	4. (b)	5. (a)	5. (b)	6. (a)	6. (b)	$\left(\frac{A(R)}{A(10)}\right)_{\text{average}}$	$f^{1f_{7/2}1/2}(R)$
8					(1,6)	1.67					(2,7)	1.81	1.74	1.51
9	(4,1)	1.24	(7,2)	1.25	(1,8)	1.31					(2,9)	1.40	1.30	1.28
10	(4,1)	1.00	(8,3)	1.00	(2,9)	1.00	(3,2)	1.00	(9,2)	1.00	(3,9)	1.00	1.00	1.00
11	(5,1)	0.65	(10,4)	0.64	(3,10)	0.62	(4,3)	0.61	(11,3)	0.70	(4,10)	0.59	0.63	0.64
12	(6,1)	0.27	(12,4)	0.26	(4,11)	0.24	(5,3)	0.25	(12,3)	0.29	(5,11)	0.23	0.26	0.27
13	(7,2)	0.077	(14,4)	0.072	(6,11)	0.066	(6,3)	0.070	(14,4)	0.084	(6,12)	0.063	0.072	0.082
14	(8,2)	0.018	(16,4)	0.016	(7,12)	0.015	(7,4)	0.016	(16,4)	0.019	(8,12)	0.014	0.016	0.020

The calculation is for the $1f_{7/2}\,1/2$ -proton state in ^{40}Ca, polarized from ^{16}O; the barrier was chosen of two center oscillator form. Columns (a) list the locations (n',ℓ') of the six different extrema appearing in the polarization contour map (ch. IV.2). Columns (b) give, for each of the extrema, the value of the polarization amplitude $A^{1f_{7/2}1/2}_{n'\ell'j'}$, divided by its value for the same extremum at R = 10 fm distance. Averages for this quantity and the function $f^{1f_{7/2}1/2}(R)$ as calculated from eq. (17) are also listed.

Figure Captions.

Fig. 1: Two Center Potentials for $^{40}Ca + ^{16}O$ at grazing distance R = 10 fm.

The potentials are shown along the z-axis.

Curve "a" is a two center Woods-Saxon potential, formed by adding Woods-Saxon potentials for the individual nuclei. The potential parameters were fitted to yield the proper binding for the $1f_{7/2}$- and $1p_{1/2}$- proton states, respectively, which are at - 1.087 MeV and - 12.11 MeV.[17,18] (r_0 = 1.2 fm; a = 0.65 fm; $V_{^{40}Ca}$ = - 57.72 MeV; $V_{^{16}O}$ = - 60.35 MeV).[19]

Curve "b" is a two center oscillator potential, with frequency parameters adjusted to the rms - radii[2] (^{40}Ca: $\hbar\omega$ = 10.90 MeV $\hat{=}$ $\sqrt{\langle r^2 \rangle}$ = 3.38 fm;[20] ^{16}O: $\hbar\omega$ = 13.00 MeV $\hat{=}$ $\sqrt{\langle r^2 \rangle}$ = 2.68 fm)[21]

The levels (full lines) are for the oscillator shell model (spin-orbit parameter $\varkappa$ = 0.08; $\underset{\sim}{l}^2$-force parameter μ = 0 for both nuclei).[14] Dashed lines indicate experimental level positions. The zero of the two center oscillator has been adjusted such that the $1f_{7/2}$ - proton state around the ^{40}Ca - core appears at the experimental position. The relative position of the $1p_{1/2}$ - proton level in ^{16}O is reproduced well.

Curve "c" is the same as "b", except that the two center oscillator barrier has been rounded off. The barrier parameter ε = 0.8 was chosen so that the barrier seen by the $1f_{7/2}$ - proton state around the ^{40}Ca - core would be close to the more realistic two center Woods-Saxon barrier, curve "a". It is seen that the rounding off

slight
also produces a/distortion of the potential away from oscillator form near the centers of the nuclei. This distortion changes with distance R. Hence, for quantities which we want to study as a function of R, we have also made calculations without the rounding off.

All calculations for $^{40}Ca + ^{16}O$ have been made with the frequency, $\underset{\sim}{\ell}\cdot\underset{\sim}{s}$- and $\underset{\sim}{\ell}^2$--parameters as given above.

Fig. 2: Polarization of the $1f_{7/2\ 1/2}$ -proton state in ^{40}Ca, due to ^{16}O.

Amplitudes for polarization by a ^{16}O - nucleus, calculated from eqs. (8), are displayed as contour maps. Also shown are amplitudes at extrema and for some strong states, notably the asymptotic state $1f_{7/2\ 1/2}$ ($\hat{=}$ $n' = 0, \ell' = 3, j' = j'_>$). Units along the contours for this and the following maps are 10^{-2}. The barrier was chosen to be the unmodified two center oscillator (i.e. $\varepsilon = 1$, cusp in the potential; see fig. 1). It is seen that the amplitude of the asymptotic state decreases as R decreases, while the amplitudes of admixed states increase. It is also evident that upon letting R become smaller the general shape of the contours persist, while all structures move towards smaller n', ℓ' (compare also table 3).

Fig. 3: Polarization of the $1f_{7/2\ 1/2}$ -proton state in ^{40}Ca, due to ^{16}O at grazing distance.

A contour map of polarization amplitudes is shown for a "realistic" choice of the barrier region ($\varepsilon = 0.8$, rounded; see fig. 1) at grazing distance R = 10 fm.

The amplitudes are similar to those for the two center oscillator at R = 10 fm; see last map of fig. 2.

Fig. 4: Polarization of the $1f_{7/2\ 3/2}$ -proton state in ^{40}Ca due to ^{16}O at grazing distance.

The same as fig. 3, but for the $\Omega = 3/2$ - component. Comparing amplitudes along contour lines it is seen that the polarization is much weaker than for $\Omega = 1/2$. The rather strong admixture of the $2p_{3/2\ 3/2}$ -state (amplitude - 0.1756) is due to the distortion of the potential near the center of the ^{40}Ca - nucleus, because of the rounding off of the barrier (compare curves "b" and "c" of fig. 1). It does not reflect a polarization effect. The actual polarization is $1 - 0.9736^2 - 0.1756^2 = 2.13$ % (generalizing eq. (13)), compared to 20.1 % for the $\Omega = 1/2$ - component (see table 2).

Fig. 5: Polarization of the $2p_{3/2\ 1/2}$ -proton state in ^{40}Ca due to ^{16}O at grazing distance.

The same as fig. 3, but for the $2p_{3/2\ 1/2}$ - state.

Fig. 6: Polarization of the $1p_{1/2\ 1/2}$ -proton state in ^{16}O due to ^{40}Ca at grazing distance.

The same as fig. 3, but for the $1p_{1/2\ 1/2}$ -proton state in ^{16}O, polarized from ^{40}Ca at R = 10 fm distance. The expansion eq. (3) was made here on tha basis of

asymptotic ^{16}O - states. All amplitudes were multiplied with $(-)^{\ell'}$, to eliminate the alternation in sign which occurs because the admixtures here are in the negative z - region, as seen from the ^{16}O - nucleus (compare fig. 1). Due to the strong binding of the $1p_{1/2}$ - state in ^{16}O, which is reproduced well in our model (cf. fig. 1), the polarization is weak, namely $1 - 0.9943^2 = 1.14$ %. In proton transfer reactions $^{40}Ca(^{16}O,^{15}N)^{41}Sc$ the polarization in the entrance channel will therefore be negligible compared to that in the exit channel (see also fig. 15).

Fig. 7: $1p_{1/2\ 1/2}$ -proton state in ^{16}O on a ^{40}Ca - basis at grazing distance.

The state shown here is identical to that of fig. 6. The difference being that the expansion eq. (3) here is made on the basis of asymptotic ^{40}Ca - states, 10 fm away from where the state is centered. The accuracy of the calculation may be seen from the fact that the normalization (cf. eq. (11)) turns out to be $1 - 3\times10^{-8}$, although no single state contributes more than $0.14^2 = 0.0196$.

Fig. 8: $1s_{1/2\ 1/2}$ -proton state in ^{16}O on a ^{40}Ca - basis at R = 12 fm distance.

At R = 12 fm the polarization of the deep lying $1s_{1/2}$ - state in ^{16}O is very weak, namely 0.12 %. The contour lines show what an essentially undisturbed $1s_{1/2}$ - state in ^{16}O looks like when expanded on the basis of ^{40}Ca - states centered at R = 12 fm distance. We find the normalization to be $1 - 7\times10^{-7}$, with no single state contributing more than $0.1229^2 = 0.015$. The missing probability is probably "real", i.e. due to the cutoff for $N' = 2n' + \ell' \leq 39$, rather than to numerical inaccuracies.

Fig. 9: Probability density of $1f_{7/2\ 1/2}$ -proton state in ^{40}Ca, polarized from ^{16}O at various distances.

Shown are contour maps for $|\psi_{1f_{7/2}\nu_2}|^2$, calculated from eq. (1) for simplicity rather than from eq. (3). The barrier was chosen to be that of the two center oscillator, to avoid the R - dependent potential distortions from the rounding off. The state at R = 16 fm is equal to the asymptotic state within line thickness. When R decreases probability around the center of the polarizing ^{16}O - nucleus builds up, the shape of which persists when R varies. At the same time the state gets weaker near the ^{40}Ca - center. For R = 10 fm an appreciable distortion near the ^{40}Ca - center is apparent. The last three maps depict the same state as fig. 2.

Figs. 10 - 12: Probability densities of polarized states.

Probability densities of $1f_{7/2\ 1/2}$-, $1f_{7/2\ 3/2}$-, and $2p_{3/2\ 1/2}$- proton states in ^{40}Ca, polarized from ^{16}O at grazing distance R = 10 fm (realistic barrier: $\varepsilon = 0.8$, rounded). The states are the same as those for which polarization amplitudes are shown in figs. 3 - 5. For comparison we have also given contour maps for the states at R = 14 fm distance of the ^{16}O - nucleus, at which the polarization is very weak (it is visible as a slight distortion of the outermost contour line, corresponding to $|\psi|^2 = 10^{-5}$, for the $2p_{3/2\ 1/2}$ - state). The admixtures for the $1f_{7/2\ 3/2}$ - state are much weaker than those for the $1f_{7/2\ 1/2}$ - state, because the former is localized off the z - axis and hence misses the polarizing ^{16}O - nucleus.

Fig. 13: Polarization of various proton states in ^{40}Ca, as a function of the distance of the polarizing ^{16}O -nucleus.

Polarization strengths as calculated from eq. (13) are shown for a number of ^{40}Ca - proton states. The barrier was chosen to be of two center oscillator form, to avoid effects from potential distortion due to rounding off (see caption to figs. 1, 4). It is seen that the polarization decreases fast with increasing R, with increasing binding ($P^{1f_{7/2}1/2} > P^{1d_{3/2}1/2} > P^{2s_{1/2}1/2}$), and with increasing Ω ($P^{1f_{7/2}1/2} > P^{1f_{7/2}3/2} > P^{1f_{7/2}5/2}$).

Fig. 14: Various polarization amplitudes for the $1f_{7/2}\ 1/2$ -proton state in ^{40}Ca, as a function of the distance of the polarizing ^{16}O -nucleus.

A selection of amplitudes showing different radial dependence (part of them may be read off from fig. 2). The barrier was chosen to be of two center oscillator form, for the same reason as in fig. 13.

Fig. 15: Dependence of Polarization on Single Particle Energy.

Polarization strengths as calculated from eq. (13) are shown for single particle proton states in ^{40}Ca and ^{16}O up to E = 52.5 MeV. The barrier was chosen "realistic" ($\mathcal{E}$ = 0.8, rounded), with ^{40}Ca and ^{16}O at grazing distance R = 10 fm. The polarization increases by roughly an order of magnitude in going to the next major shell. The energy dependence follows the same pattern in ^{40}Ca (polarized from ^{16}O) as it does in ^{16}O (polarized from ^{40}Ca). Resonance effects for the mutual polarization of the $2s_{1/2}$ - and $1d_{3/2}$ - ^{16}O - states and the $1f_{7/2}$ - and $2p_{3/2}$ - ^{40}Ca - states are clearly visible (compare also table 2).

Fig. 16: Polarization Effects on Single Particle Energies in the system $^{40}Ca + ^{16}O$.

Single particle energies for a number of ^{16}O - and ^{40}Ca - proton states are shown as a function of distance R. The barrier was chosen to be of two center oscillator form, for the same reason as in figs. 13, 14. The crosses at R = 10 fm indicate single particle energies for a "realistic" barrier ($\varepsilon = 0.8$, rounded). They are seen to be pushed up by roughly 1 MeV, because of the distortion of the potential due to the rounding off (compare curves "b" and "c" in fig. 1).

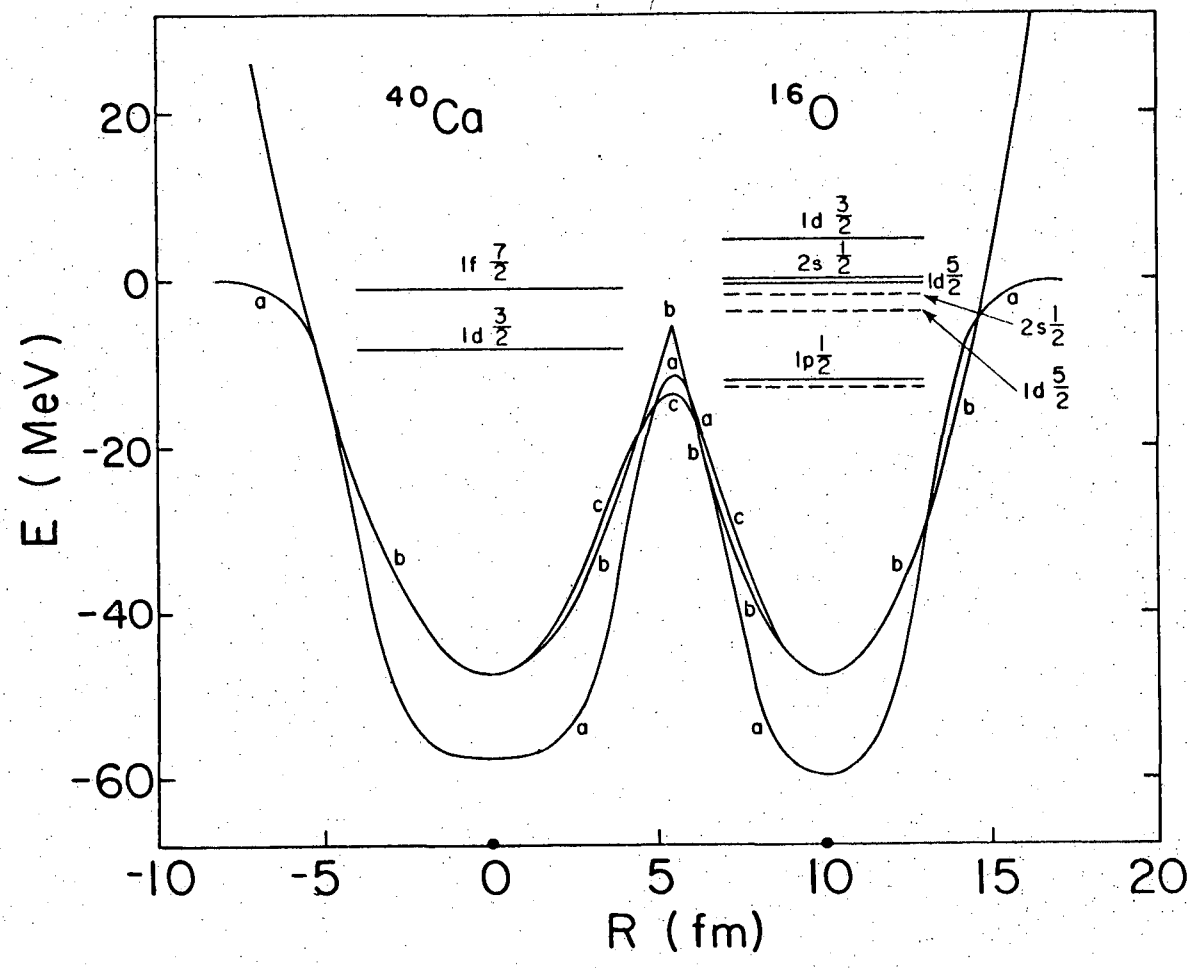

Fig. 1: Two Center Potentials for ^{40}Ca + ^{16}O at grazing distance R = 10 fm.

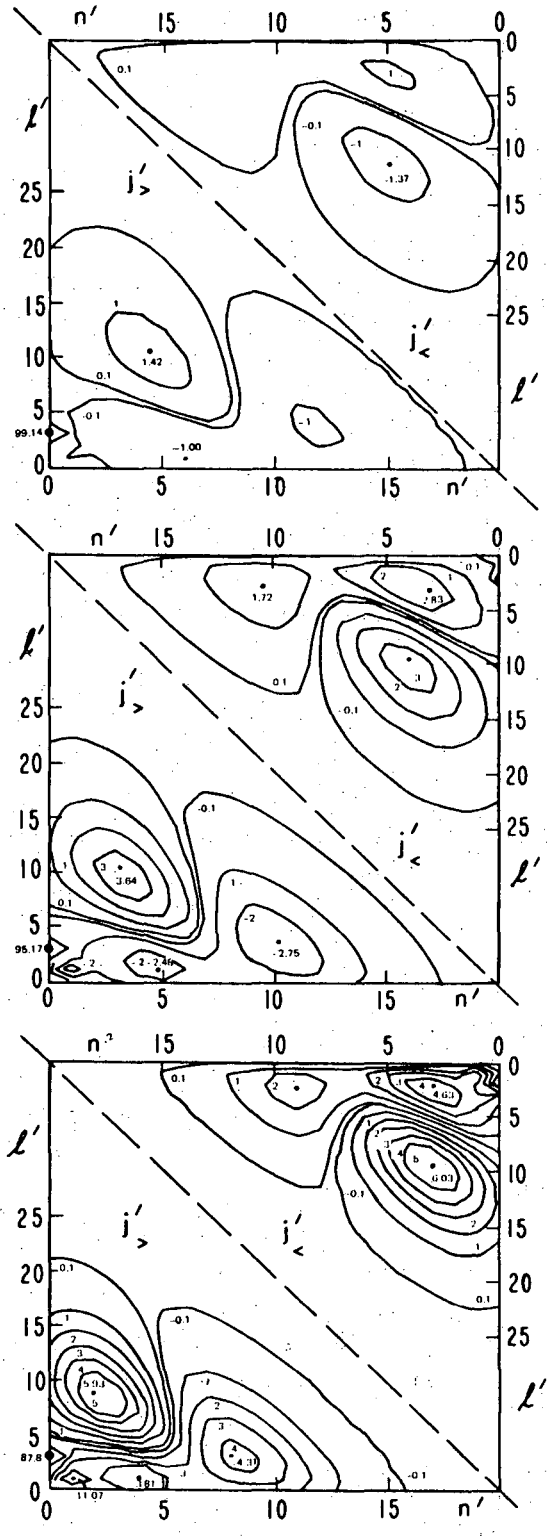

Fig. 2: Polarization of the $lf_{7/2\ 1/2}$ -proton state in ^{40}Ca, due to ^{16}O.

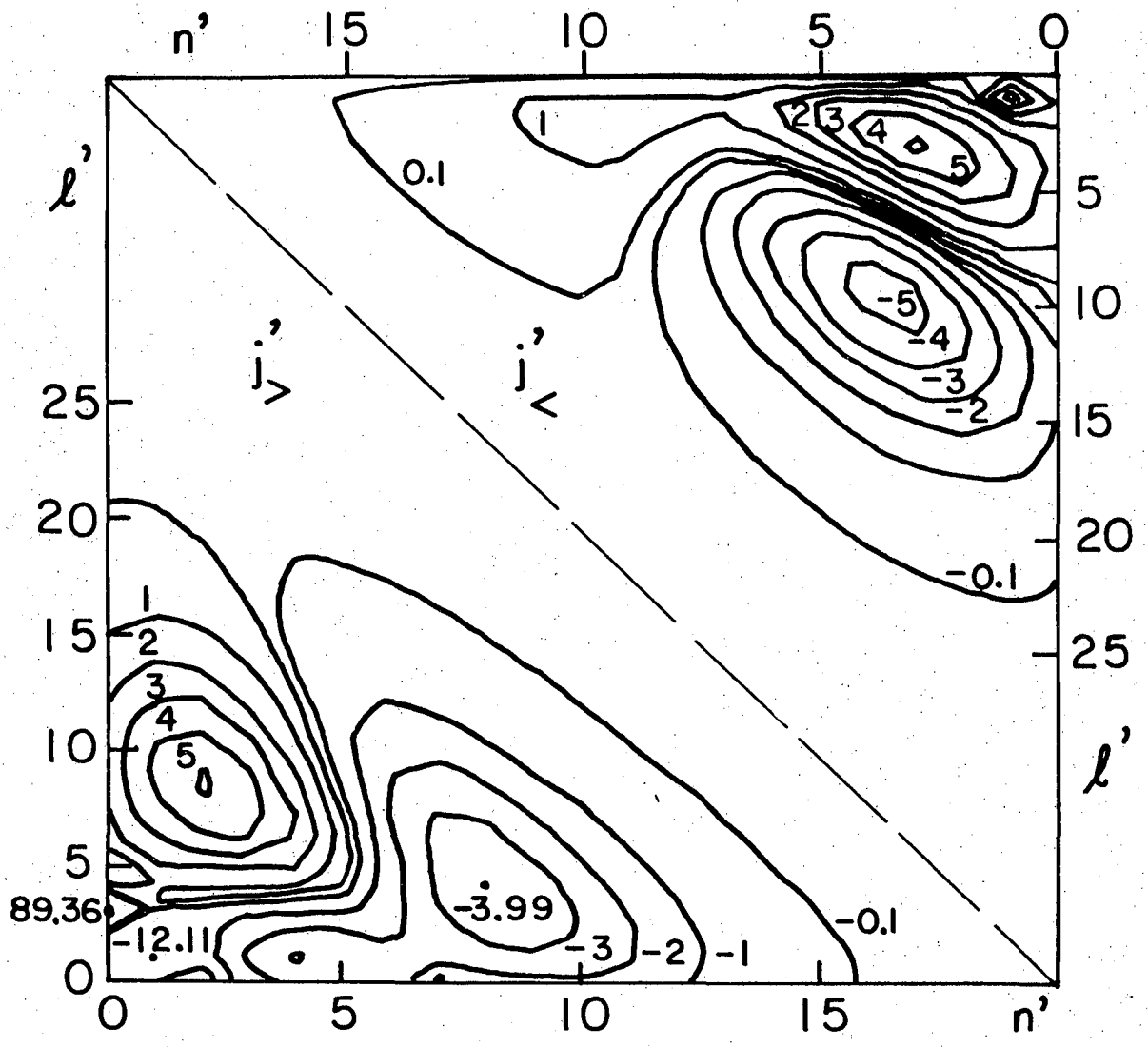

Fig. 3: Polarization of the $1f_{7/2\ 1/2}$ -proton state in ^{40}Ca, due to ^{16}O at grazing distance. (R = 10 fm, ε = 0.8r)

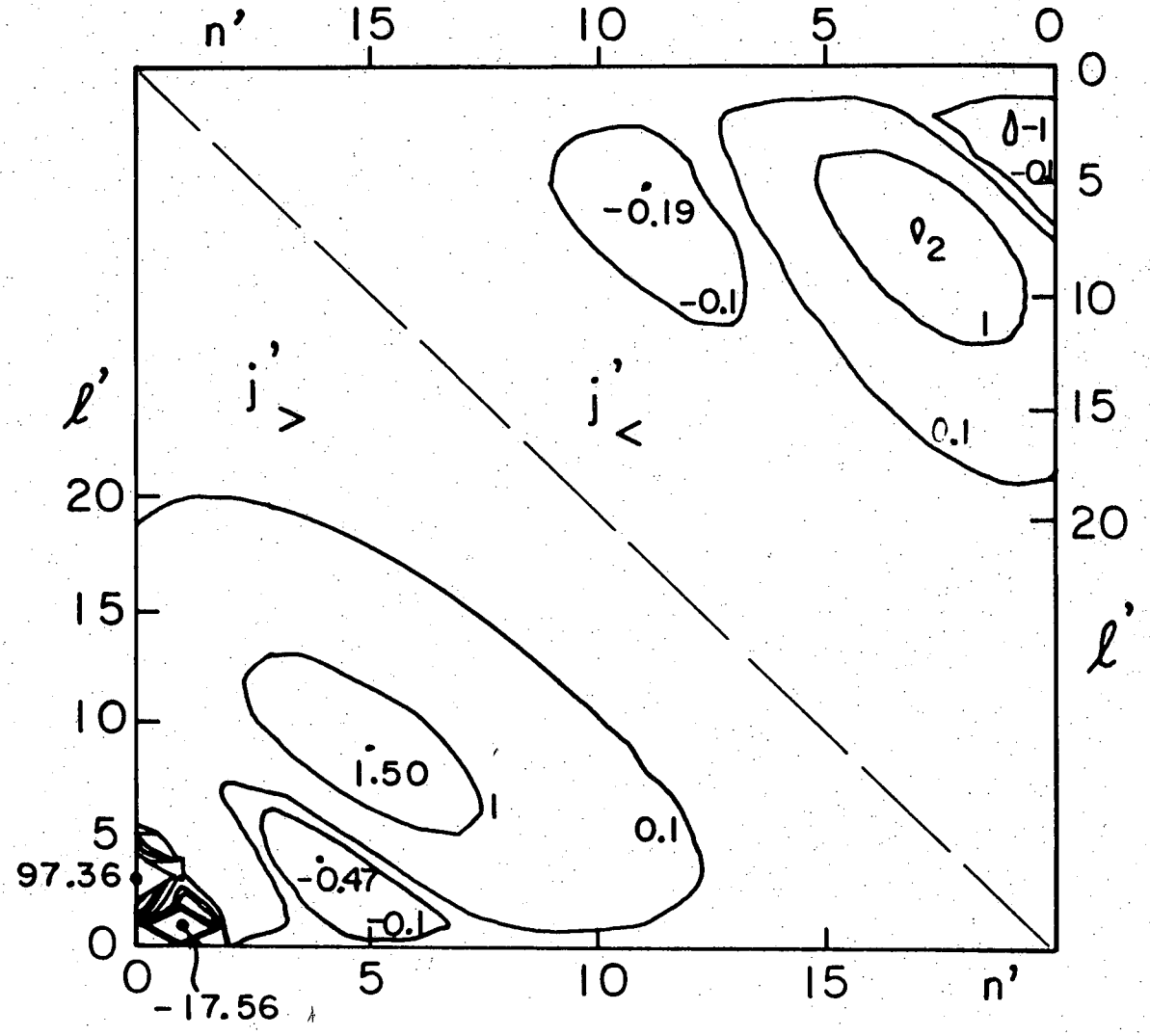

Fig. 4: Polarization of the $1f_{7/2\ 3/2}$ -proton state in ^{40}Ca due to ^{16}O at grazing distance. (R = 10 fm, ε = 0.8r)

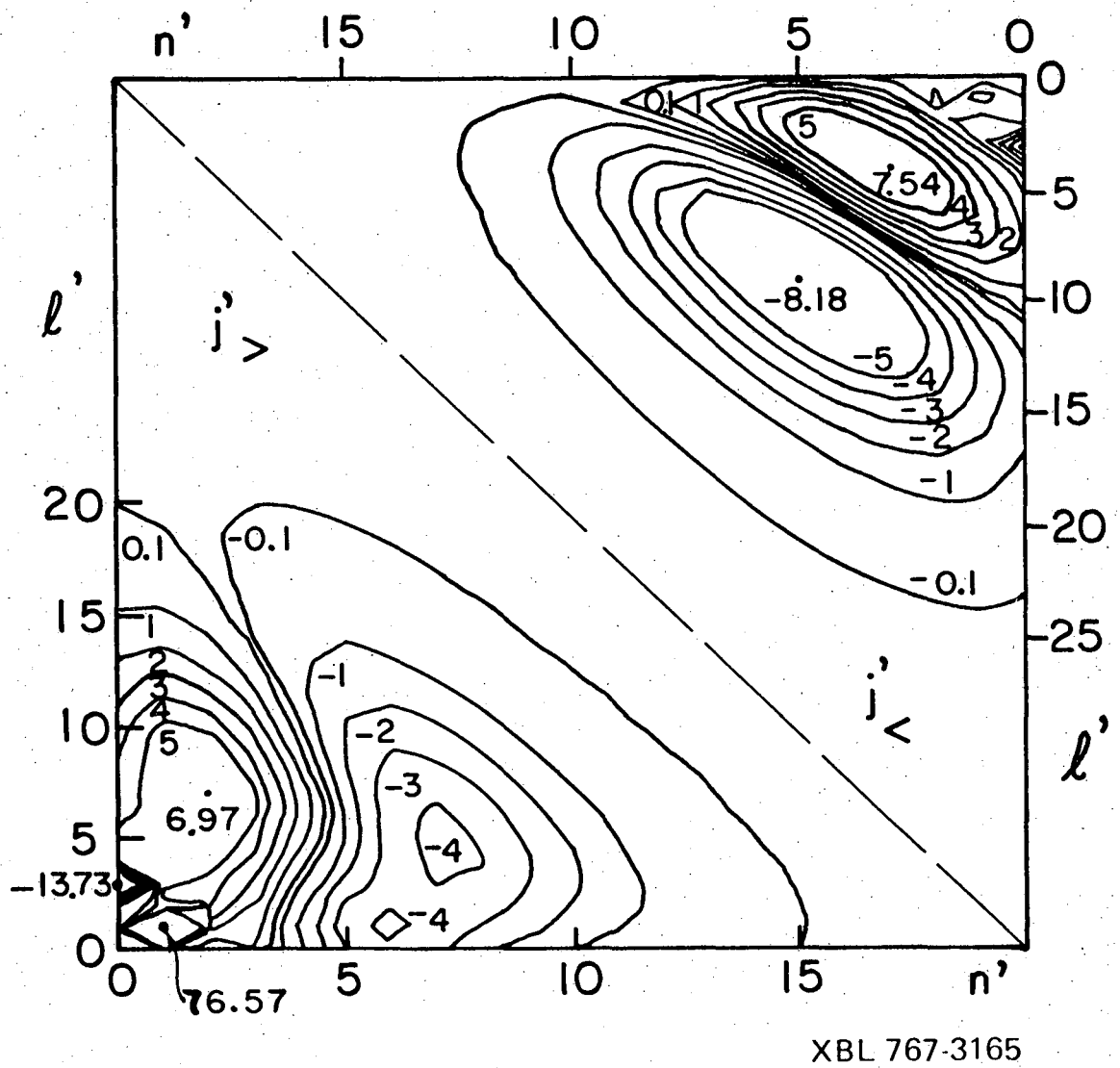

Fig. 5: Polarization of the $2p_{3/2\ 1/2}$ -proton state in ^{40}Ca due to ^{16}O at grazing distance. (R = 10 fm, ε = 0.8r)

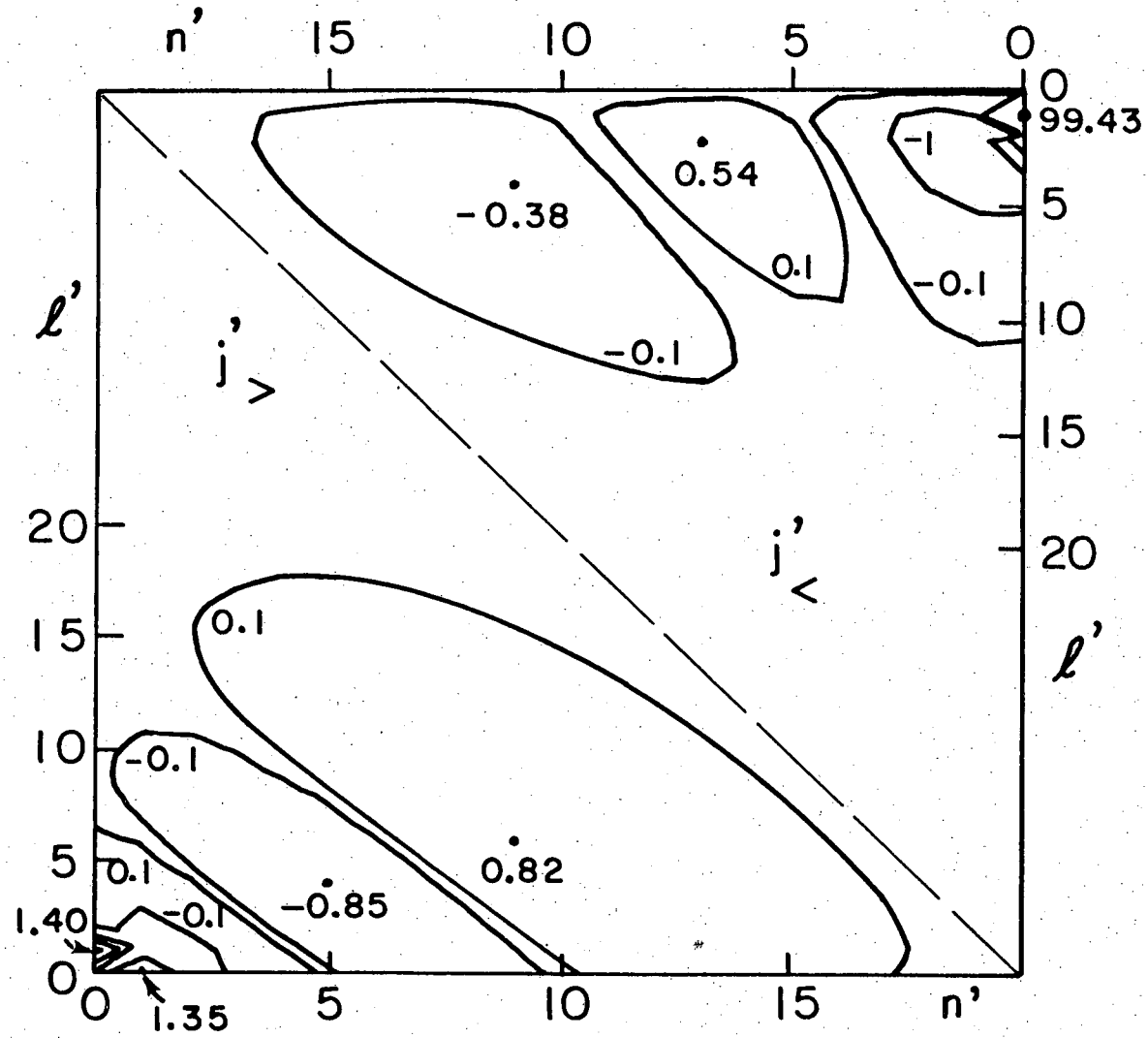

XBL 767-3161

Fig. 6: Polarization of the $1p_{1/2\ 1/2}$ -proton state in ^{16}O due to ^{40}Ca at grazing distance. (R = 10 fm, ε = 0.8r)

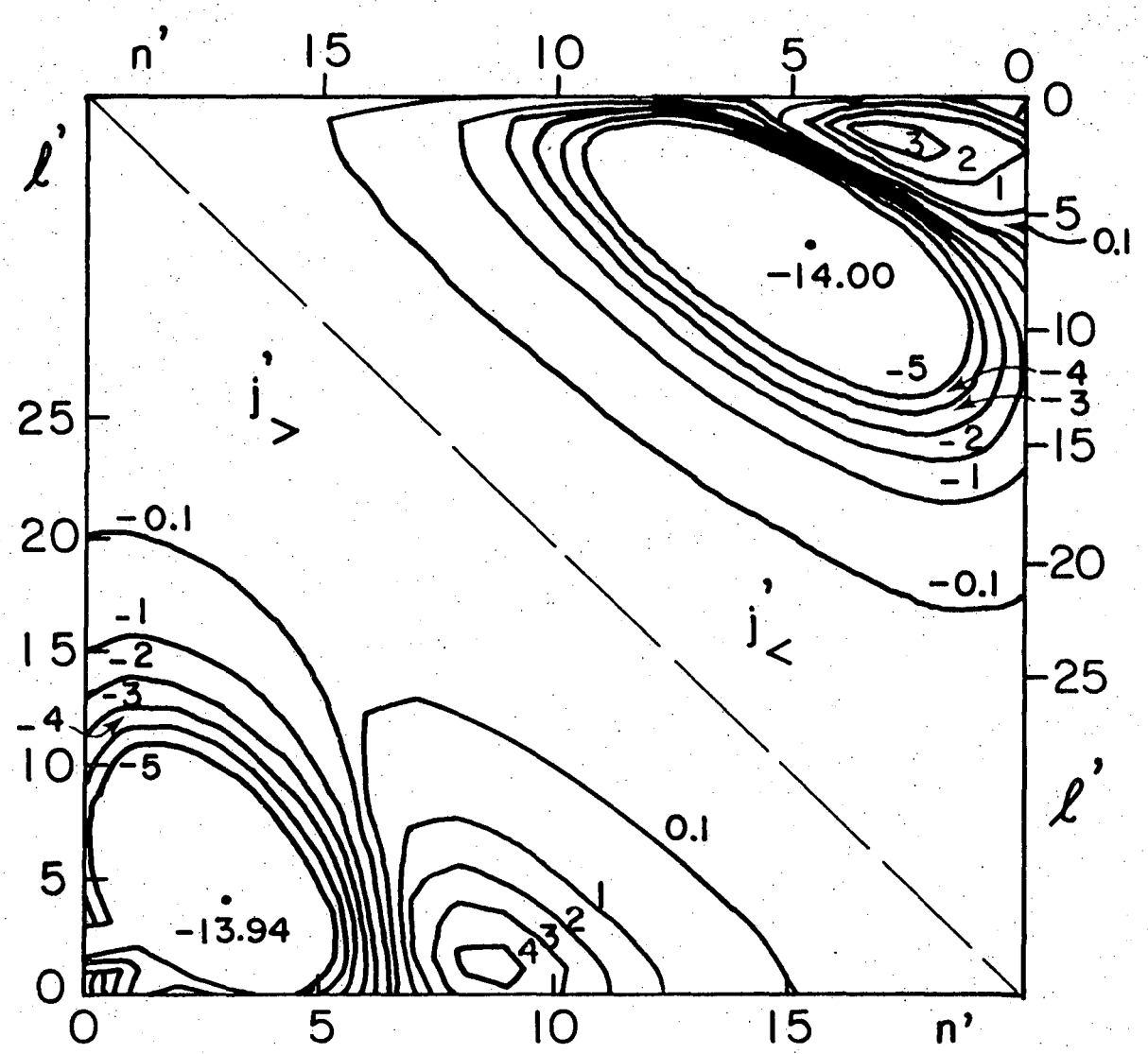

Fig. 7: $1p_{1/2\ 1/2}$ -proton state in ^{16}O on a ^{40}Ca -basis at grazing distance.

(R = 10 fm, ε = 0.8r)

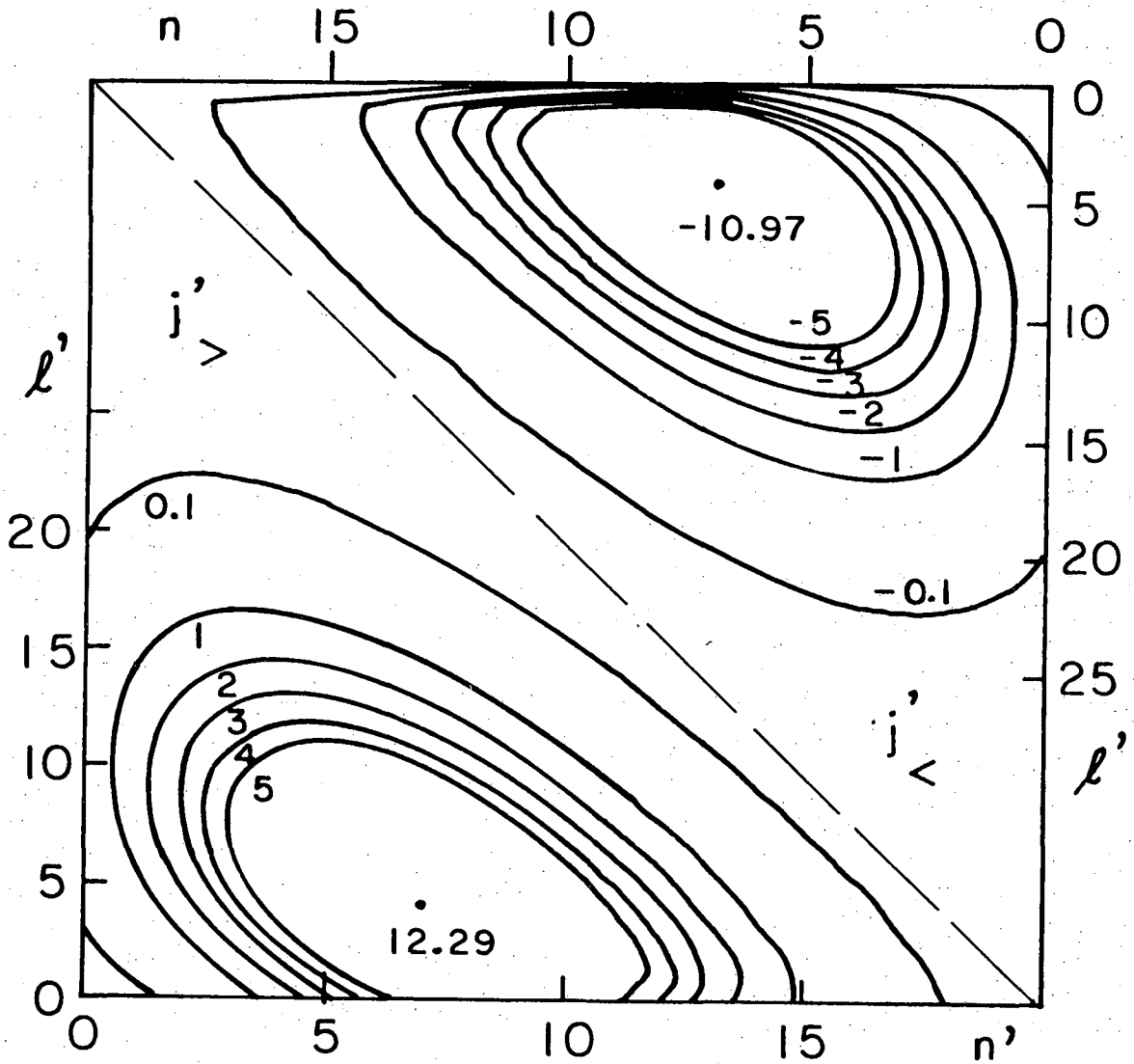

XBL 767-3159

Fig. 8: $1s_{1/2\ 1/2}$ -proton state in ^{16}O on a ^{40}Ca -basis at R = 12 fm distance.

(R = 12 fm, ε = 0.8r)

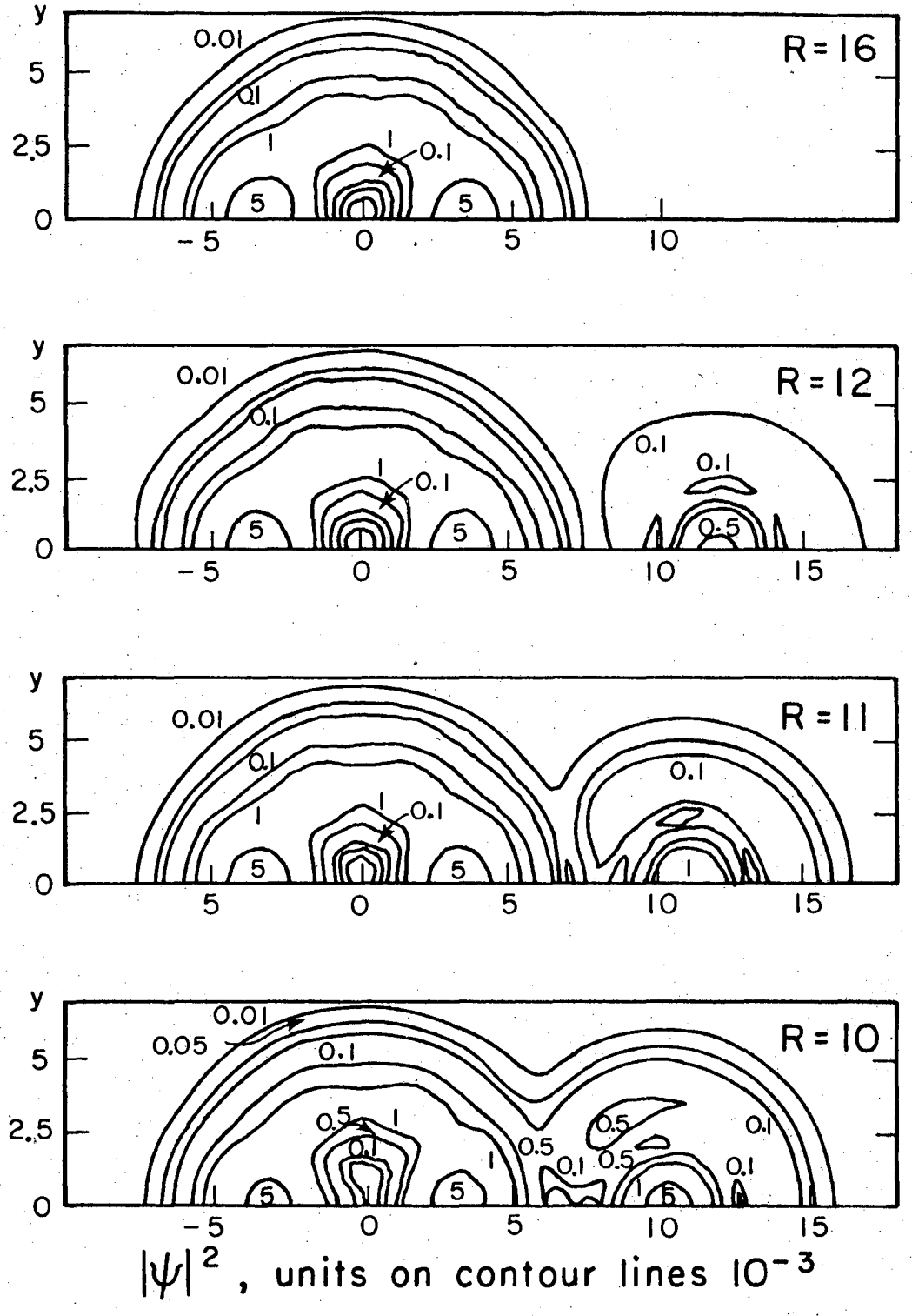

XBL 766-2944

Fig. 9: Probability density of the $1f_{7/2\ 1/2}$ -proton state in ^{40}Ca, polarized from ^{16}O at various distances. (R in fm, $\mathcal{E}$ = lc)

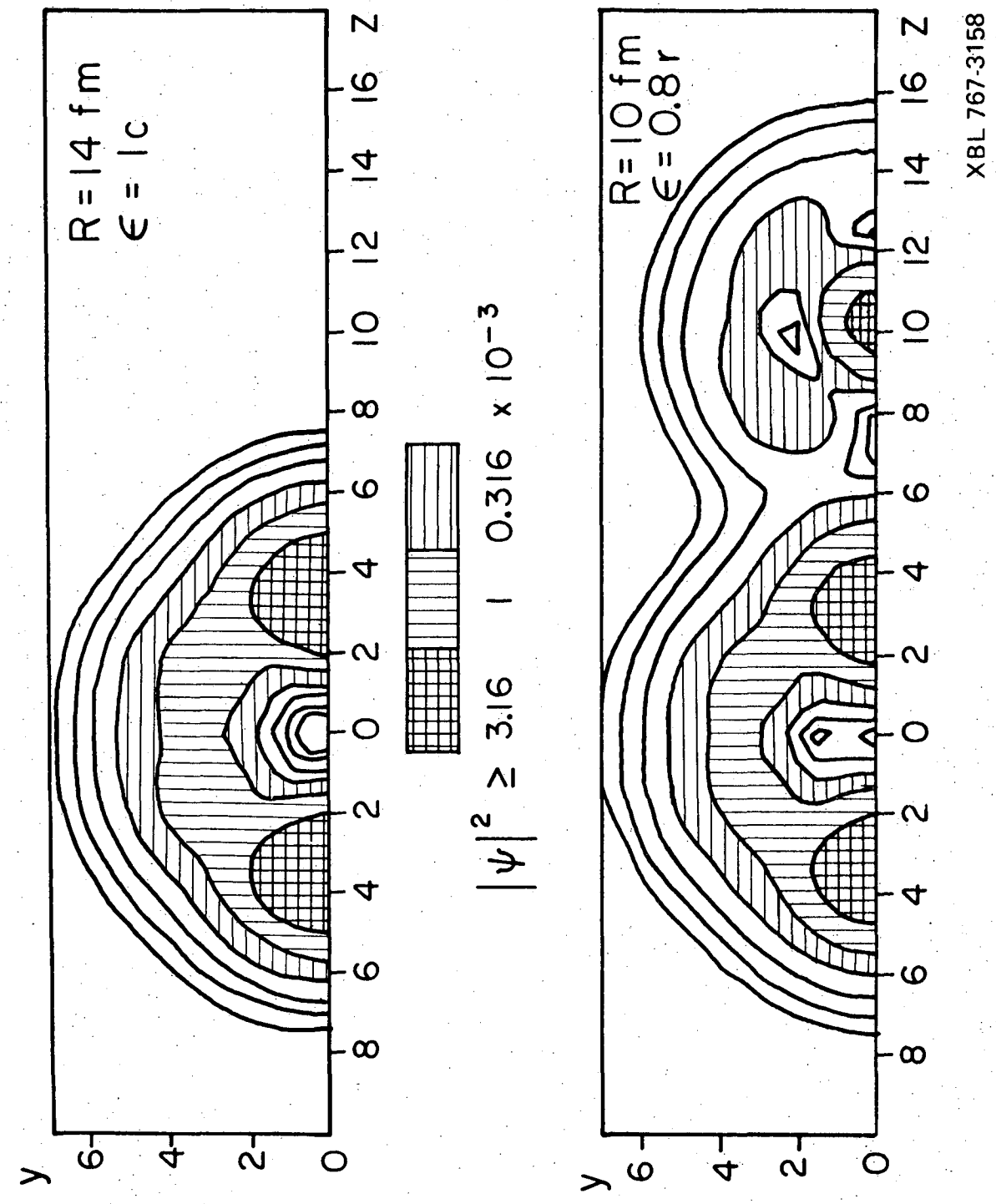

Fig. 10: Probability density of the $1f_{7/2\ 1/2}$ -proton state in ^{40}Ca, polarized from ^{16}O under nearly asymptotic (R = 14 fm, ε = 1c) and under grazing (R = 10 fm, ε = 0.8r) conditions.

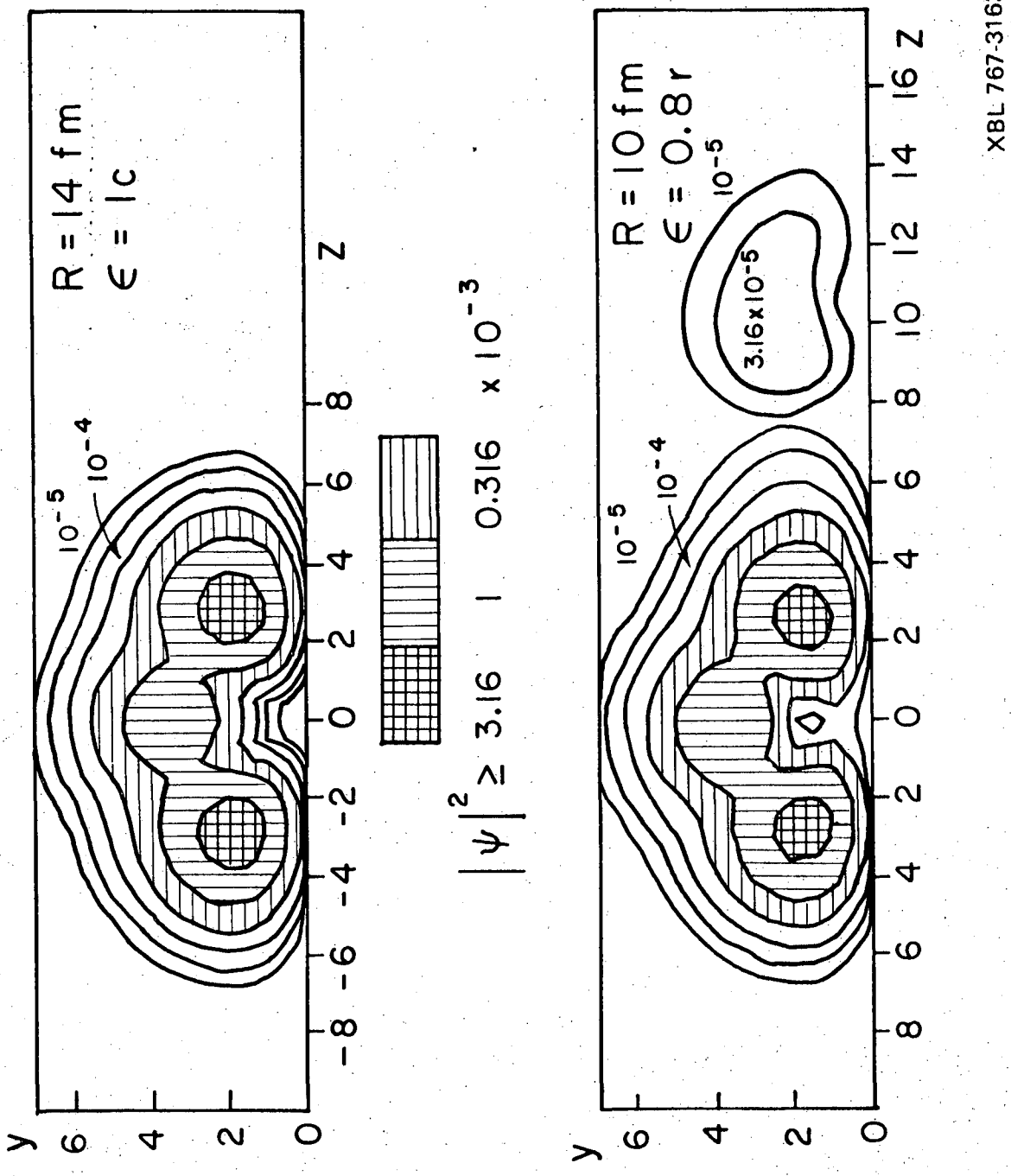

XBL 767-3163

Fig. 11: Probability density of the $1f_{7/2\ 3/2}$ -proton state in ^{40}Ca, polarized from ^{16}O under nearly asymptotic (R = 14 fm, ε = 1c) and under grazing (R = 10 fm, ε = 0.8r) conditions.

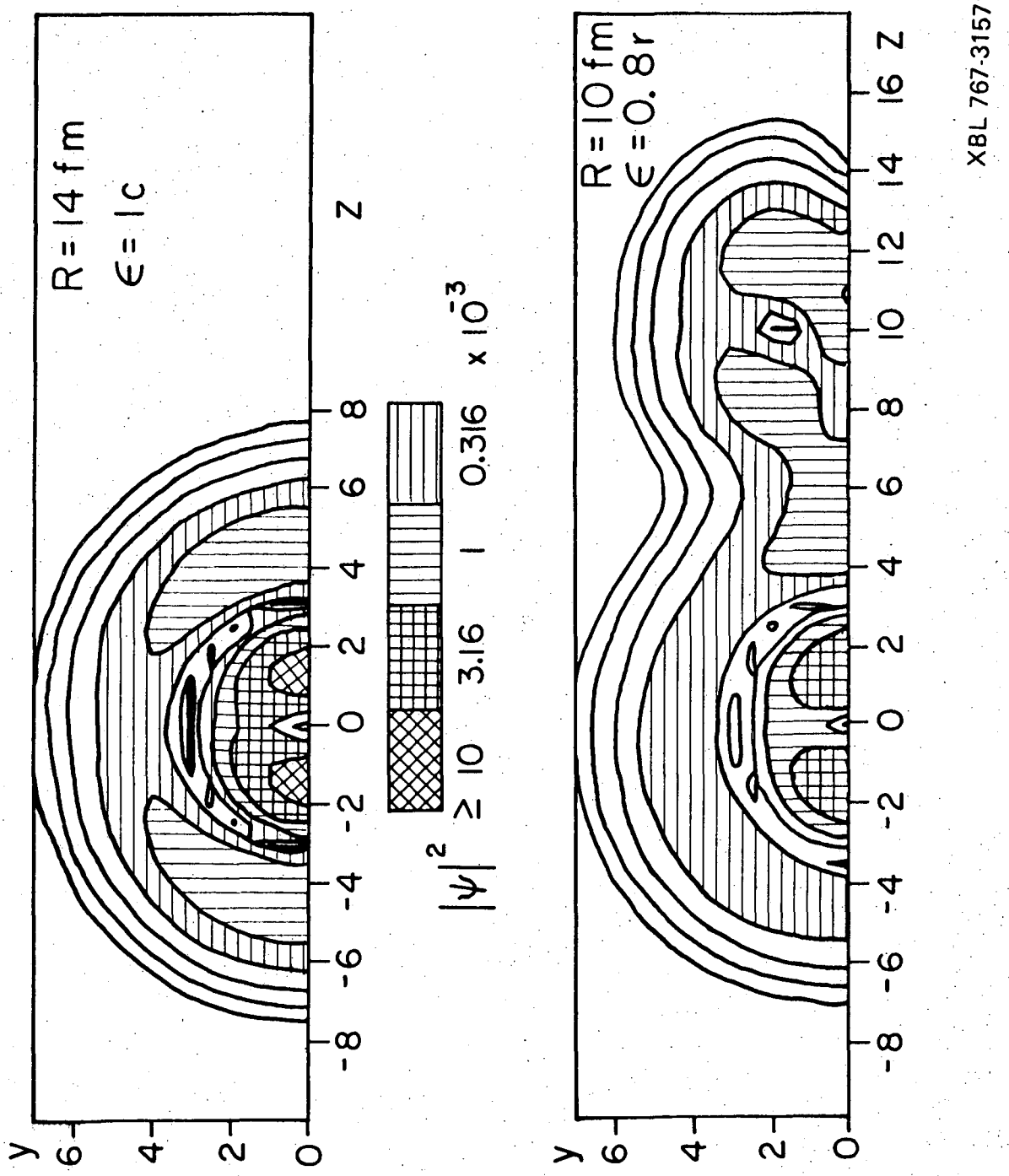

Fig. 12: Probability density of the $2p_{3/2\ 1/2}$ -proton state in ^{40}Ca, polarized from ^{16}O under nearly asymptotic (R = 14 fm, $\boldsymbol{\varepsilon}$ = 1c) and under grazing (R = 10 fm, $\boldsymbol{\varepsilon}$ = 0.8r) conditions.

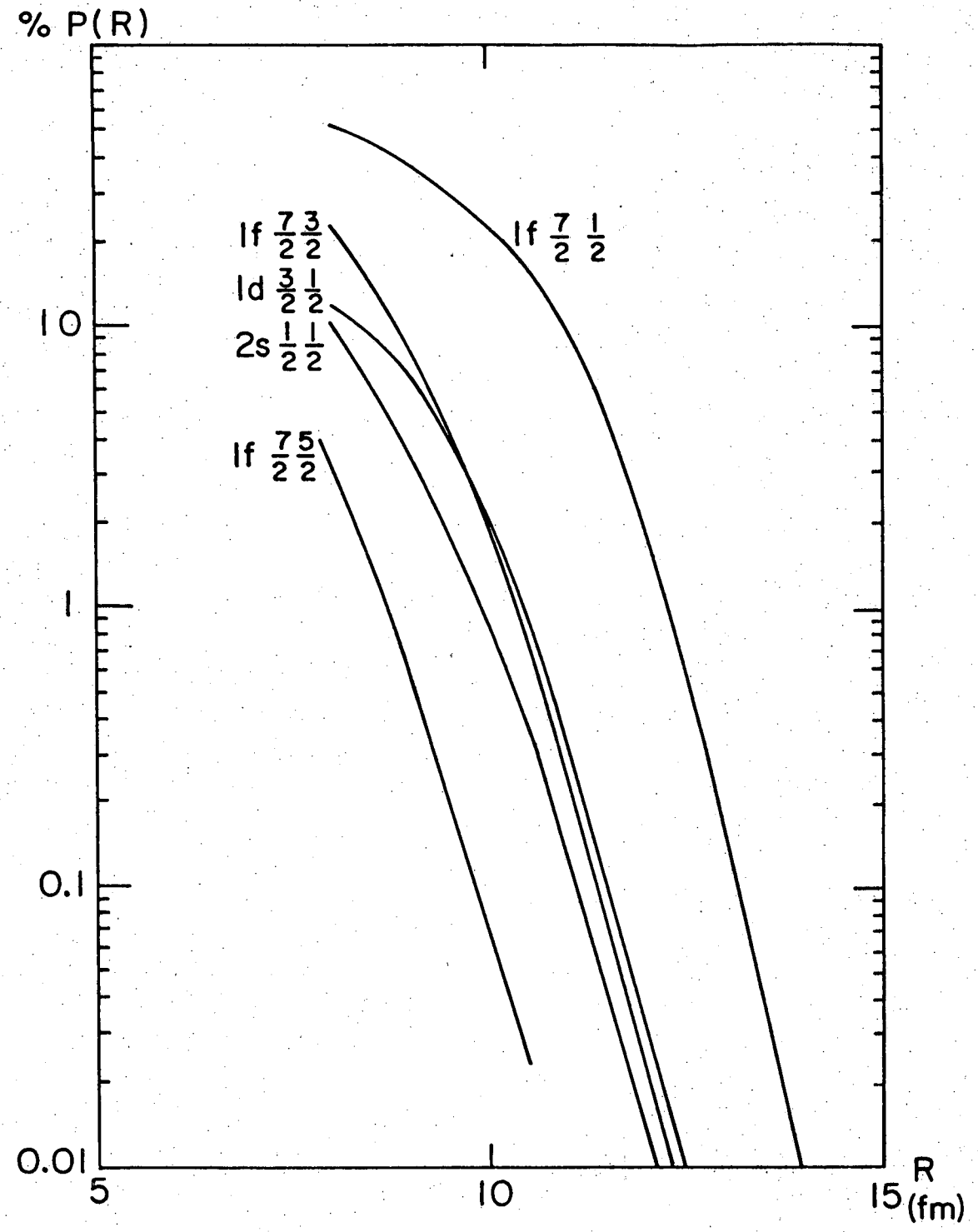

XBL 766-2943

Fig. 13: Polarization of various proton states in ^{40}Ca, as function of the distance of the polarizing ^{16}O -nucleus.

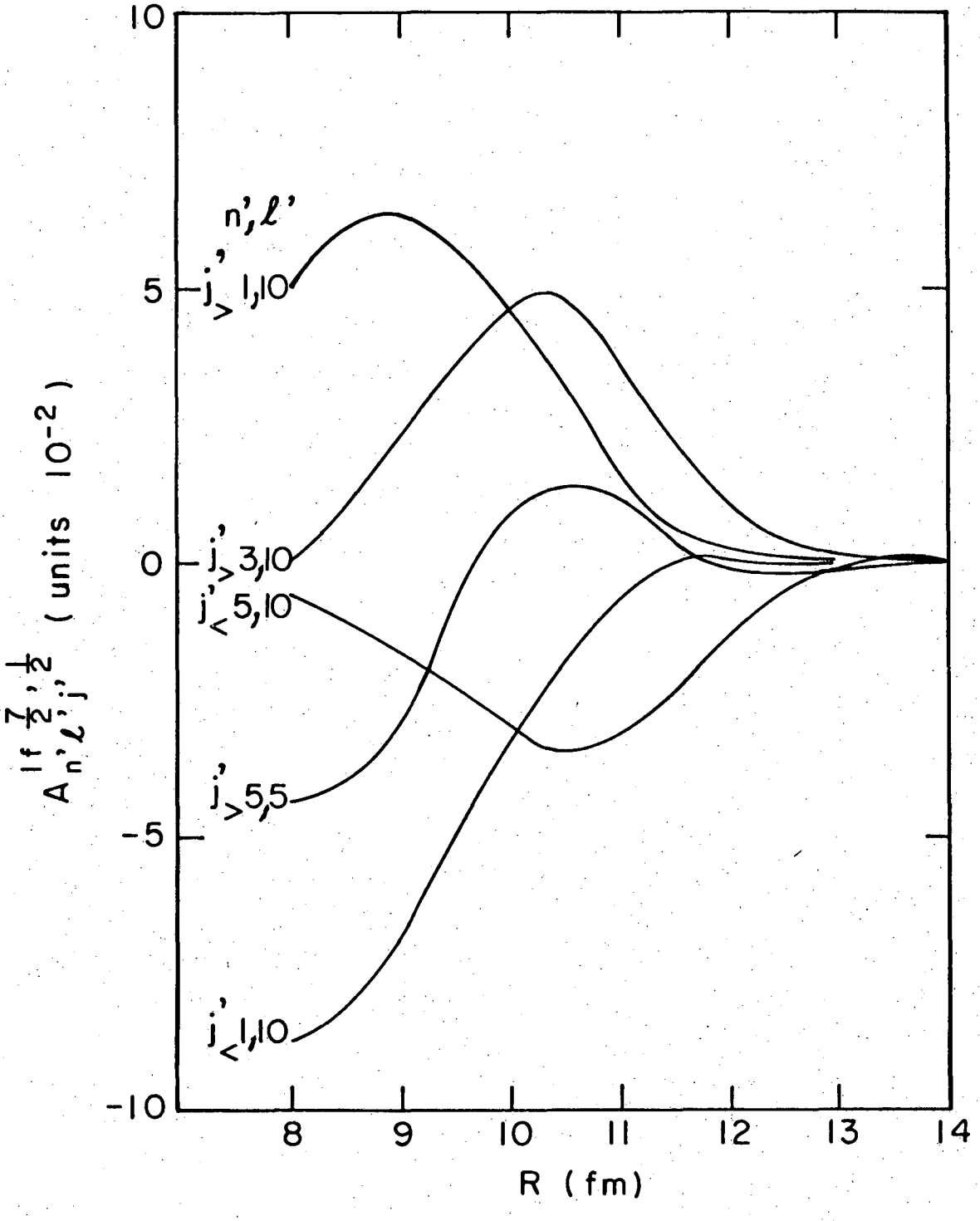

XBL 767-3186

Fig. 14: Various polarization amplitudes for the $1f_{7/2\ 1/2}$ -proton state in ^{40}Ca, as a function of the distance of the polarizing ^{16}O -nucleus.

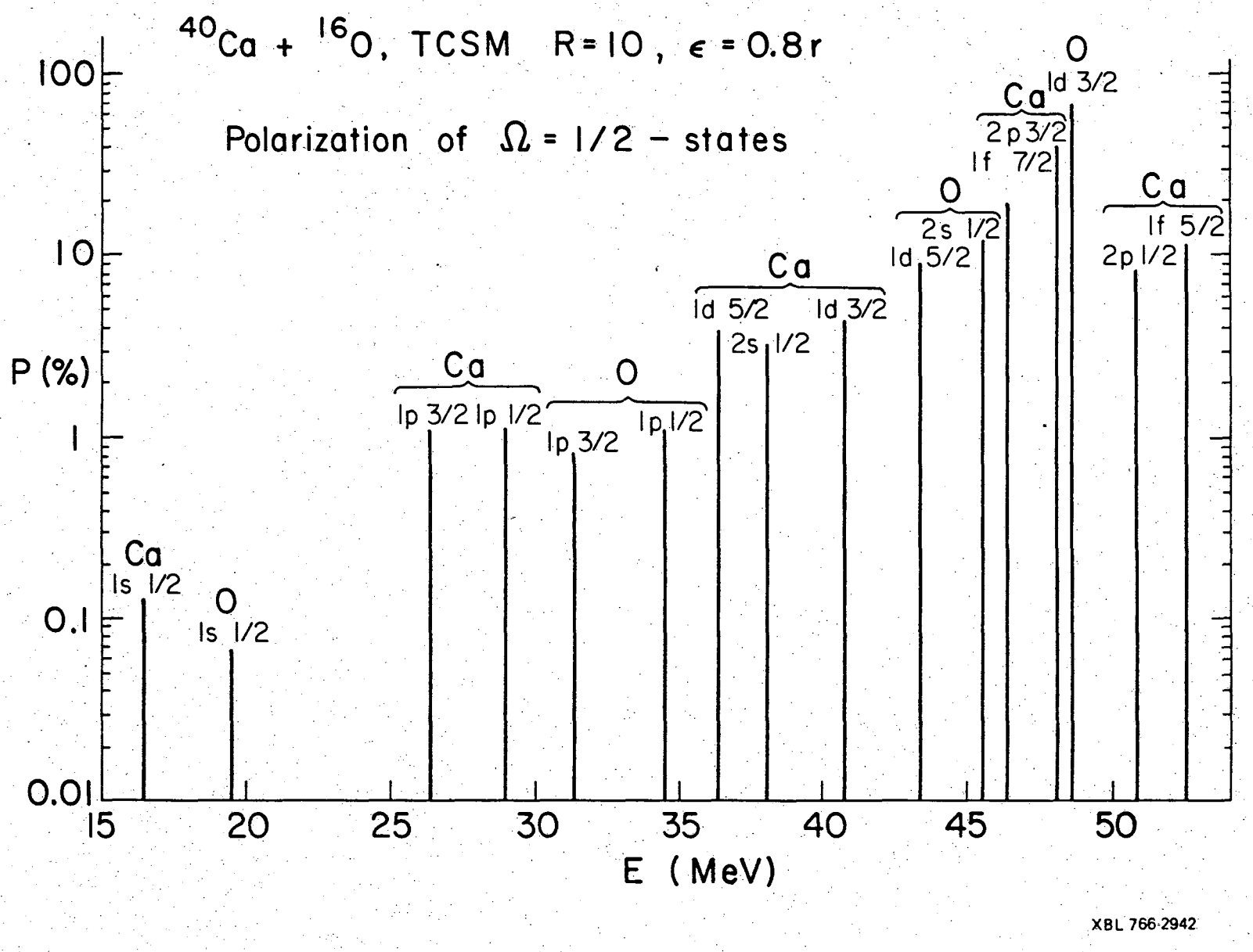

Fig. 15: Dependence of polarization on single particle energy.

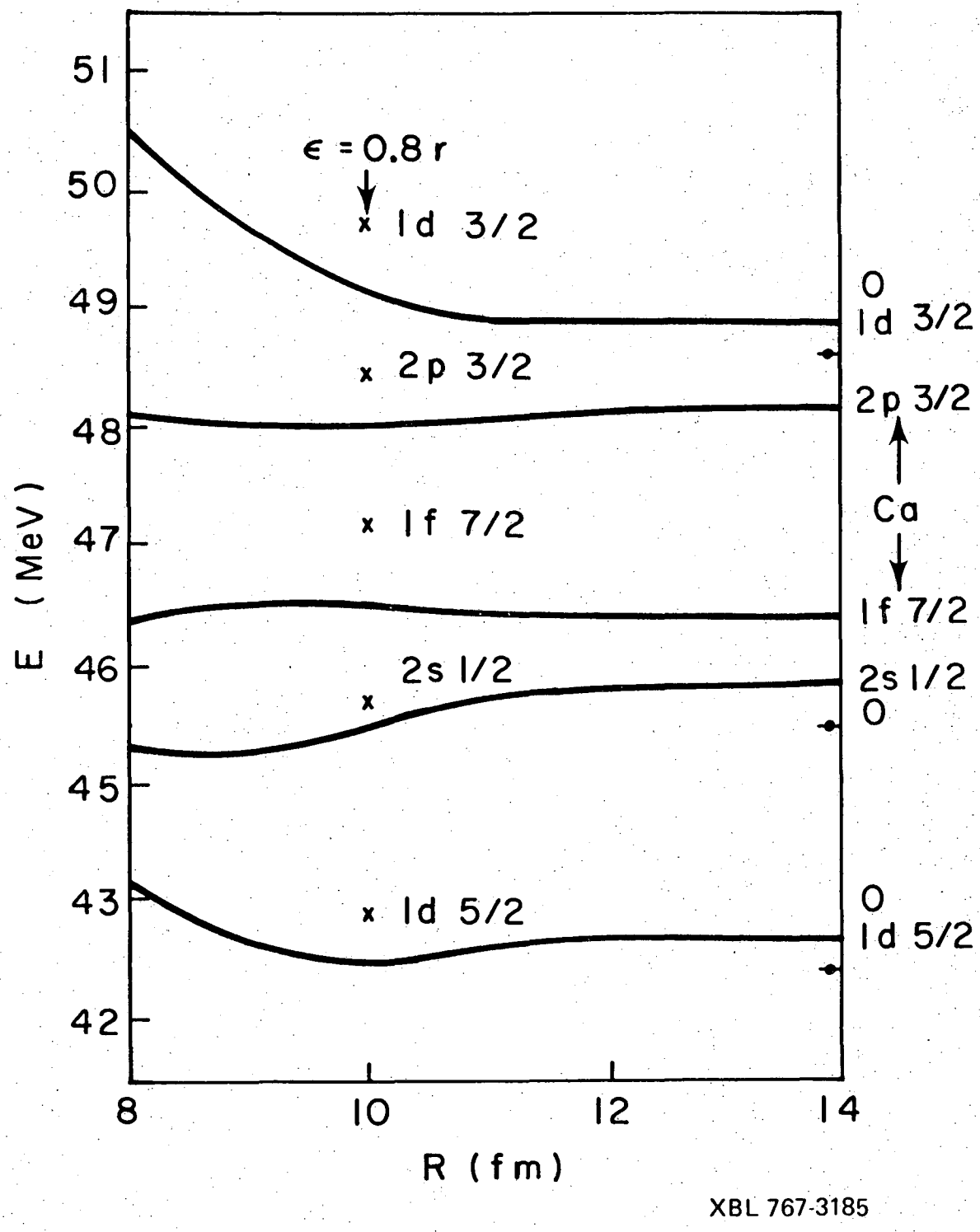

Fig. 16: Polarization effects on single particle energies in the system $^{40}Ca + ^{16}O$.

References.

1. P. Holzer, U. Mosel, and W. Greiner, Nucl. Phys. A138(1969)241.

2. K. Pruess and W. Greiner, Phys. Lett. 33B(1970)197; K. Pruess, Thesis, Frankfurt/Main 1972 (unpublished).

3. U. Mosel, T.D. Thomas, and P. Riesenfeldt, Phys. Lett. 33B(1970)565.

4. D. Scharnweber, W. Greiner, and U. Mosel, Nucl. Phys. A164(1971)257.

5. M. Rayet and G. Reidemeister, J. Physique 32, C6-259 (1971).

6. J.A. Maruhn and W. Greiner, Z. Physik 251(1972)431; J.A. Maruhn, Diploma thesis, Frankfurt/Main 1971 (unpublished).

7. T. Morovic, Thesis, Frankfurt/Main 1973 (unpublished).

8. H.C. Pauli, Phys. Rep. 7C(1973) No. 1 (and references therein).

9. T. Tazawa, Progr. Theor. Phys. 51(1974)1764.

10. H.J. Specht, Rev. Mod. Phys. 46(1974)773 (and references therein).

11. K. Pruess, G. Delic, L.A. Charlton, and N.K. Glendenning, LBL - report 5008 (presented at the Symp. on Macr. Features of Heavy Ion Collisions, Argonne/Ill., 1976); and to be published.

12. K. Pruess and P. Lichtner, LBL - report 4381, to be published in Nucl. Phys..

13. A.S. Davydov, Quantum Mechanics, Pergamon Press, Oxford 1965.

14. C. Gustafsson, Int. Conf. on the Properties of Nuclei far from the Region of Beta - Stability, Leysin, Switzerland, 1970, CERN - report 70-30, p. 654; I. Ragnarsson, ibid., p. 847.

15. W. von Oertzen, Nucl. Phys. A148(1970)529; A. Gobbi, in: Proc. Int. Conf. React. between Compl. Nucl., Nashville 1974, vol.2 p. 211.

16. M. Abramowitz, I.A. Stegun, Handbook of Mathematical Functions, Dover Publications, New York 1965.

17. J.H.E. Mattauch et al., Nucl. Phys. 67(1965)32.

18. F. Ajzenberg-Selove, T. Lauritzen, Nucl. Phys. 11(1959)1; V. Gillet and N. Vinh Mau, Nucl. Phys. 54(1964)321.

19. G. Delic, private communication.

20. T.W. Donnelly and G.E. Walker, Phys. Rev. Lett. 22(1969)1121.

21. R.W. Shaw et al., Proc. Phys. Soc. 86(1965)513.

22. P. Lichtner and K. Pruess. to be published.

23. J.D. Talman, Nucl. Phys. A141(1970)273.

This report was done with support from the United States Energy Research and Development Administration. Any conclusions or opinions expressed in this report represent solely those of the author(s) and not necessarily those of The Regents of the University of California, the Lawrence Berkeley Laboratory or the United States Energy Research and Development Administration.

TECHNICAL INFORMATION DIVISION
LAWRENCE BERKELEY LABORATORY
UNIVERSITY OF CALIFORNIA
BERKELEY, CALIFORNIA 94720